




Intra-somatosensory cortical circuits mediating pain-induced analgesia

Received: 23 May 2024

Accepted: 5 February 2025

Published online: 21 February 2025



Ji-Ye Huang^{1,6}, Yu-Xin Jin^{1,6}, Wan-Ying Dong^{1,6}, Wan Zhao^{2,6}, Ping-Kai Cheng¹, Jun-Hao Miao¹, An Liu³, Di Wang¹, Juan Li¹, Zhi Zhang^{1,4} , Wenjuan Tao^{1,3,5}  & Xia Zhu¹ 


Pain in one part of the body profoundly diminishes the sensation of pain in other parts of the body in humans. Here, we found that pain-related behaviors in hindpaw are inhibited by noxious stimuli from diverse body regions in mice. Using activity-dependent cell labeling in male *Fos*^{TRAP2} mice, we captured a neuronal ensemble in the layers 2–4 of secondary somatosensory cortex (S2) that was activated during pain at diverse body regions induced analgesia. Single-cell projection analysis showed that these S2 neurons receive projections from the contralateral S2 and specifically innervate the layer 4 of primary somatosensory cortex (S1). Microendoscopic calcium imaging and chemogenetic manipulation in freely moving mice showed that this S2 → S1 feedforward inhibitory circuit mediates ipsilateral pain-induced analgesia, whereas contralateral S2 innervation of the S2 → S1 circuit mediates contralateral pain-induced analgesia. Our study defines the intra-somatosensory cortical circuits underlying “pain inhibiting pain”, expanding the scope of known circuit mechanisms involved in pain relief.

Studies in healthy humans have demonstrated that a remotely applied noxious “conditioning” stimulus inhibits a subject’s pain response to a “test” stimulus^{1–3}. This phenomenon wherein pain experienced in one body region can inhibit pain in another body region was termed as conditioned pain modulation (CPM) in humans and was first discovered in 1979 and termed as Diffuse noxious inhibitory controls (DNIC) in animals^{4,5}. Previous research into the mechanism(s) of DNIC have predominantly focused on the role of descending projections from the brainstem to the spinal cord, including opioidergic and noradrenergic projections^{6–8}. Of note, top-down control from higher-order structures, such as the cerebral cortex, is known to modulate the intensity of pain perception by inhibiting or facilitating the transmission of nociceptive

information^{9–12}. The mechanisms by which these higher brain structures that mediate “pain-inhibiting pain” still unclear.

The somatosensory cortex network has been reported to be involved in memory and decision-making^{13,14}. Inhibition of the somatosensory cortex impairs motor memory retention and behaviorally relevant decision coding^{15,16}. The somatosensory cortex is also involved in context-dependent sensory processing^{17,18}. Recent research on the primary somatosensory cortex (S1) across species has revealed the existence of clear laminar contributions underlying sensory input^{19–21}. The secondary somatosensory cortex (S2), as a higher-order cortical area, processes somatosensory stimuli based on experience, and its response correlates with perceptual behavior²², suggesting that S2-related cortical networks play a role in the conversion of sensory input

¹Department of Anesthesiology and Pain Medicine, The First Affiliated Hospital of USTC, Center for advance interdisciplinary science and biomedicine of IHM, Division of Life Sciences and Medicine, University of Science and Technology of China, Hefei, PR China. ²Department of Otolaryngology-Head and Neck Surgery, The First Affiliated Hospital of University of Science and Technique of China, Hefei, PR China. ³Department of Physiology, School of Basic Medical Sciences, Anhui Medical University, Hefei, PR China. ⁴Department of Biophysics and Neurobiology, CAS Key Laboratory of Brain Function and Disease, University of Science and Technology of China, Hefei, PR China. ⁵College & Hospital of Stomatology, Anhui Medical University, Key Laboratory of Oral Diseases Research of Anhui Province, Hefei, PR China. ⁶These authors contributed equally: Ji-Ye Huang, Yu-Xin Jin, Wan-Ying Dong, Wan Zhao.

 e-mail: zhizhang@ustc.edu.cn; wjtao01@ahmu.edu.cn; xiaozhu@ustc.edu.cn

into perception²³. The role of the somatosensory cortex in subjective sensory experiences supports the likely involvement of somatosensory crosstalk in the “pain-inhibiting pain”.

In the present study, we combined viral tracing, activity-dependent genetic labeling, microendoscopic calcium imaging, and optogenetic manipulations to ultimately discover internal circuits between the S2 and S1 that underlie pain-induced analgesia. Nociceptive threshold behavioral tests showed that noxious stimuli elicited by a pinch or capsaicin injection in the ipsilateral forepaw, contralateral forepaw, or cheek all inhibited pain-related behaviors in hindpaw. We subsequently found that noxious stimuli applied to ipsilateral forepaw activates projections from layers 2–4 of S2 specifically to layer 4 GABAergic neurons in SIHL (SIHL^{GABA}), which in turn drives inhibition of local glutamatergic neurons in SIHL (S2 → SIHL^{GABA} → SIHL^{Glu} feed-forward inhibitory circuit) to mediate analgesia in the hindpaw. By contrast, noxious stimuli applied to contralateral forepaw activates the contralateral S2 which, through interhemispheric communication with S2, activates an inhibitory circuit in SIHL to mediate analgesia of hindpaw. These findings reveal that the S2 → S1 circuit and the contralateral S2 innervation of S2 → S1 circuit respectively mediate ipsilateral or contralateral pain-induced analgesia, expanding the scope of our understanding of the circuit basis of pain relief.

Results

Pain at diverse body regions induces analgesia

To determine whether pain could inhibit pain in other parts in mice, we first established an inflammatory pain model by injecting the left hindpaw with Complete Freund's adjuvant (CFA, 1 mg/ml, 10 μ l) (Supplementary Fig. 1a). Routine nociceptive threshold assays conducted at 3 days post-injection showed that CFA group mice displayed significantly decreased nociceptive thresholds in the inflamed left hindpaw compared to the controls (Supplementary Fig. 1b). We next examined whether noxious stimuli by pinching^{24,25} in other anatomical regions could inhibit pain-related behavior in the inflamed hindpaw by applying an alligator clip to the left forepaw of the CFA 3 d mice. In mice with inflamed left hindpaw, pinching of the left forepaw resulted in significantly increased nociceptive thresholds compared to no-pinch control mice (alligator clips taped to the left forepaw). Specifically, elevated nociceptive thresholds were detected in the von Frey tests (i.e., increased mechanical sensitivity thresholds), a hot plate tests (i.e., increased the latency for lick responses), a brush tests (i.e., decreased dynamic score), and spontaneous pain tests (i.e., decreased spontaneous pain score), and this effect diminished by 20 min after removal of the pinch stimulus (Fig. 1a, b and Supplementary Movie 1). These results suggested that noxious stimuli applied to left forepaw induce analgesia in the left hindpaw.

To assess whether pinch stimuli in anatomical regions other than the ipsilateral forepaw can also inhibit pain-related behavior in the left hindpaw, we applied a pinch stimulus to the right forepaw or cheek, which are each known to have ascending sensory information pathways distinct from that of the left forepaw^{26,27}. Similarly, nociceptive thresholds of the inflamed hindpaw were significantly increased following pinch stimuli compared with that in the respective forepaw or cheek no-pinch controls, and this effect again diminished within 20 min of clip removal (Supplementary Fig. 1c–f).

To investigate whether noxious stimuli other than mechanical pinch can elicit analgesic effects in the hindpaw, we applied an alternative intense noxious stimulus by injecting different concentrations of the TRPV1 channel agonist capsaicin²⁸, including 1 μ g/10 μ l, 5 μ g/10 μ l, and 10 μ g/10 μ l into the left forepaw of CFA mice. We found that 1 μ g/10 μ l capsaicin did not result in significantly elevated nociceptive thresholds in the inflamed hindpaw of CFA mice (Supplementary Fig. 2a, b). In contrast, 5 μ g/10 μ l or 10 μ g/10 μ l capsaicin dosages led to significantly increased nociceptive thresholds, and this inhibition of pain-related behaviors persisted for at least 4 h after administering the

10 μ g/10 μ l capsaicin injection (Fig. 1c, d and Supplementary Fig. 2c, d). We therefore selected 10 μ g/10 μ l as the capsaicin dosage in all subsequent experiments. We also injected capsaicin into the right forepaw or the cheek. Similarly, nociceptive thresholds were significantly elevated in the inflamed hindpaw following capsaicin injection, compared with that in saline-injected controls (Fig. 1e–h, Supplementary Movie 2 and 3). Given the relatively long-lasting, stable analgesic effects of capsaicin injection in the forepaw and cheek in the inflamed hindpaw of CFA mice, we employed capsaicin injections to examine pain-induced analgesia throughout the remainder of our study.

In addition, we investigated whether noxious stimulus affects the nociceptive threshold in the hindpaw of naive mice by injecting capsaicin into the left forepaw, right forepaw, or cheek. Mechanical and thermal nociceptive threshold tests of the left hindpaw indicated significantly elevated nociceptive thresholds compared to saline-injected control mice, and this effect diminished by 4 h after capsaicin injection (Supplementary Fig. 3). Together, these results demonstrated that pain-induced analgesia in both naive and CFA-induced pain model mice.

Given that the attachment of an alligator clip and capsaicin injection elicited paw-licking or face-wiping behaviors could distract mice from paying attention to their hindpaw being tested, we replaced the noxious stimulus treatment with non-noxious stimulus chloroquine (CQ, which induces scratching behavior) treatment as the second stimulus^{29,30}. We found that injecting CQ (100 μ g in 10 μ l) into the left forepaw of CFA mice resulted in a significantly increased in biting behavior (indicating an attention shift but not pain) (Supplementary Fig. 4a, b, and Supplementary Movie 4). Nociceptive threshold tests showed no significant change in the inflamed hindpaw of these CQ-treated mice (Supplementary Fig. 4c). Similarly, nociceptive thresholds of the inflamed hindpaw were not significantly increased following CQ injection into the right forepaw or cheek (Supplementary Fig. 4d–i). These results thus support that noxious stimulus applied to another body part is necessary for the observed “pain-inhibiting pain” phenomenon.

Increased neuronal activity in the secondary somatosensory cortex during pain-induced analgesia

As the somatosensory cortex is known to harbor and process pain information^{31,32}, and given our observation that noxious stimuli at diverse sites (e.g., ipsilateral forepaw, contralateral forepaw, cheek) each inhibited pain-related behavior in the hindpaw of both CFA and naive mice, we inferred that a neuronal ensemble might be present in the somatosensory cortex, responsible for pain in diverse sites and mediating pain-induced analgesia. To explore this possibility, we monitored activated neurons during pain at diverse sites induced analgesia using a reporter mouse line generated by crossing FosCreER^{T2} (*Fos*^{TRAP2}) mice, expressing tamoxifen-inducible Cre recombinase under the c-Fos promoter, with *Ail4-tdTomato* mice^{33,34}, to enable tdTomato expression in activated neurons that show *Fos* induction after intraperitoneal injection of 4-hydroxytamoxifen (4-OHT) (*Fos*^{TRAP2:Ail4} mice).

In CFA *Fos*^{TRAP2:Ail4} mice, we injected capsaicin into the left forepaw, right forepaw, or cheek after 4-OHT injection and sacrificed the mice 2 week later to examine tdTomato expression (indicative of neuronal activity) across whole-brain slices (Fig. 2a). In CFA mice with capsaicin injection in the left forepaw, tdTomato expression was significantly increased in the secondary somatosensory cortex (S2, right hemisphere, which is contralateral to the CFA injection in the left hindpaw), the forepaw region of the primary somatosensory cortex (S1FL, right hemisphere), and the contralateral S2 (contra-S2, left hemisphere), whereas it was significantly decreased in the hindpaw region of the primary somatosensory cortex (SIHL, right hemisphere, which is contralateral to the CFA injection in the left hindpaw) compared to control mice (Fig. 2b, c and Supplementary Fig. 5).

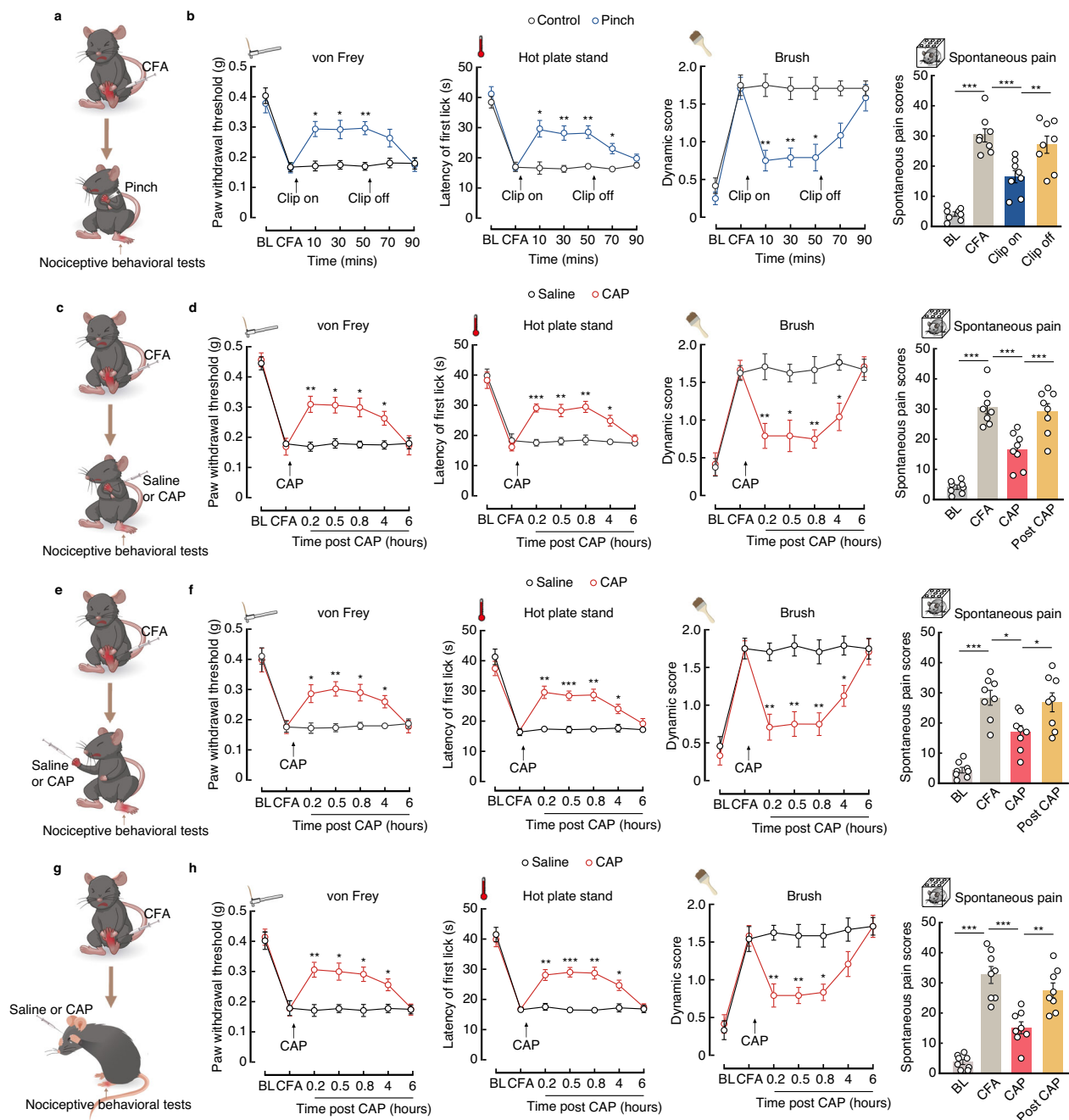
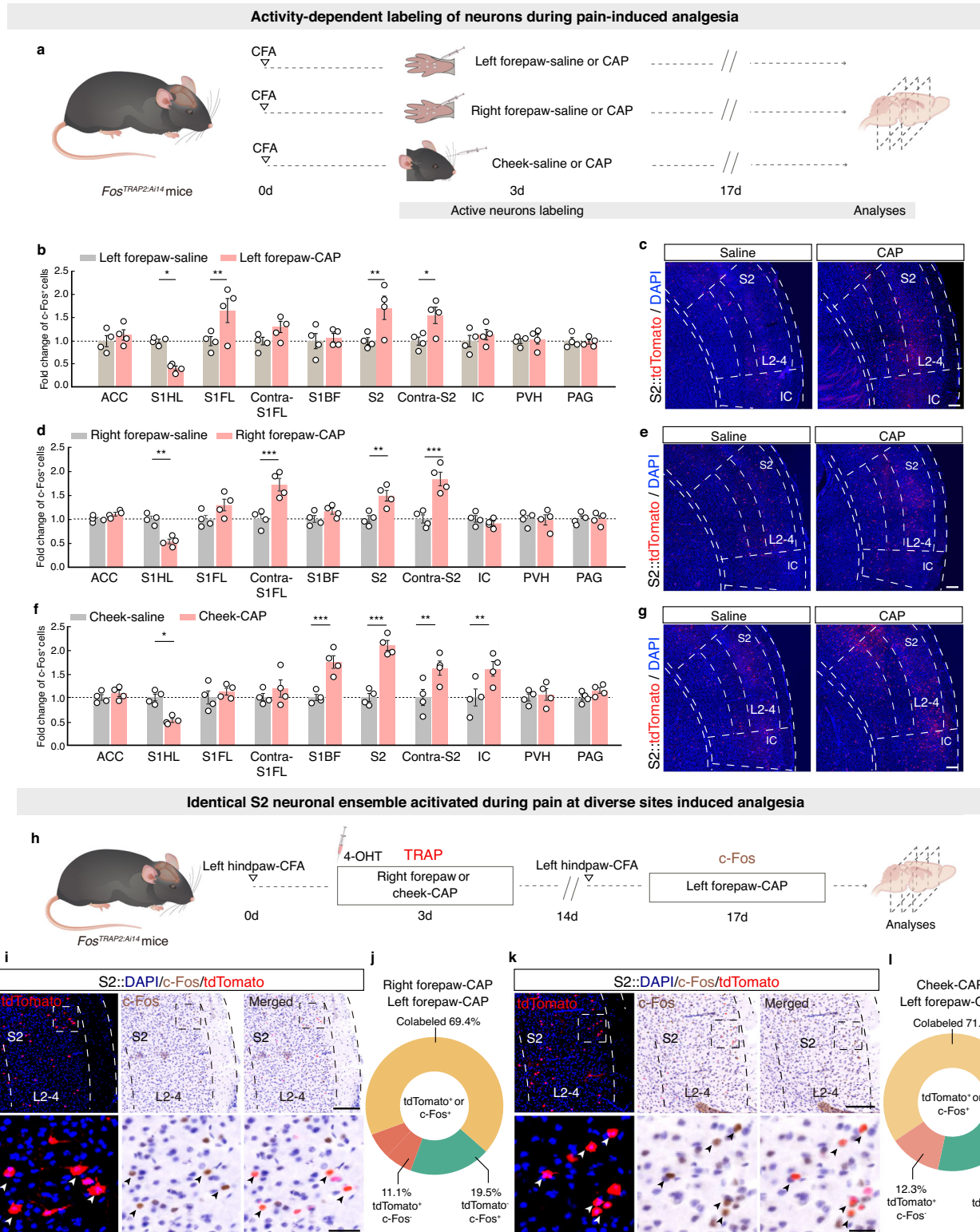


Fig. 1 | Noxious stimuli at diverse body regions induce hindpaw analgesia in mice. **a** Schematic for establishing a pain-induced analgesia model by pinch stimulus of the left forepaw in CFA mice and assessing nociceptive thresholds in the left hindpaw. **b** Time course assessment of nociceptive thresholds in the left hindpaw by the von Frey test, hot plate tests, brush tests, and spontaneous pain tests ($n = 8$ mice per group; von Frey, $F_{1,14} = 34.20$, $p < 0.0001$; Hot plate, $F_{1,14} = 46.05$, $p < 0.0001$; Brush, $F_{1,14} = 141.8$, $p < 0.0001$; Spontaneous pain, $F_{3,28} = 32.63$, $p < 0.0001$). **c–h** Schematic of CAP injection into the left forepaw (**c**), right forepaw (**e**), or cheek (**g**) in CFA mice. Time course assessment of nociceptive thresholds in the left hindpaw in CFA mice with CAP injection in the left forepaw (**d**); $n = 8$ mice per group; von Frey, $F_{1,14} = 16.97$, $p = 0.001$; Hot plate, $F_{1,14} = 34.09$,

$p < 0.0001$; Brush, $F_{1,14} = 26.74$, $p = 0.0001$; Spontaneous pain, $F_{3,28} = 38.63$, $p < 0.0001$, right forepaw (**f**; $n = 8$ mice per group; von Frey, $F_{1,14} = 27.51$, $p = 0.0001$; Hot plate, $F_{1,14} = 83.79$, $p < 0.0001$; Brush, $F_{1,14} = 40.08$, $p = 0.0001$; Spontaneous pain, $F_{3,28} = 22.87$, $p < 0.0001$), or cheek (**h**; $n = 8$ mice per group; von Frey, $F_{1,14} = 37.00$, $p < 0.0001$; Hot plate, $F_{1,14} = 83.21$, $p < 0.0001$; Brush, $F_{1,14} = 14.85$, $p = 0.0018$; Spontaneous pain, $F_{3,28} = 36.26$, $p < 0.0001$). BL, baseline; CAP, capsaicin. Significance was assessed by two-way repeated-measures ANOVA with post hoc comparison and one-way ANOVA with post hoc Bonferroni's test between groups in **b**, **d**, **f**, and **h**. Data are presented as means \pm SEM. * $P < 0.05$; ** $P < 0.01$; *** $P < 0.001$. Details of the statistical analyses are presented in Supplementary Data 2. Source data are provided as a Source Data file.

Similarly, CFA mice injected with capsaicin in the right forepaw showed a significant increase in tdTomato expression in the contralateral S1FL, S2 and the contralateral S2, but significantly decreased in S1HL (Fig. 2d, e and Supplementary Fig. 6a, b). CFA mice administered capsaicin injection in the cheek had significant increased

tdTomato expression in the insular cortex (IC), the barrel field of primary somatosensory cortex (S1BF), S2 and the contralateral S2, but also showed significantly decreased tdTomato expression in the S1HL relative to that in control animals (Fig. 2f, g and Supplementary Fig. 6c, d). These results showing increased c-Fos-expressing (TRAPed)



neurons in S2 upon pain delivery to all three examined sites (Supplementary Data 1). We found that activated neurons in S2 are enriched in layers 2–4, so we subsequently restricted our experiments to layers 2–4 of S2 for the remainder of the study (Supplementary Fig. 7). In addition, the decrease in c-Fos expression in S1HL upon pain delivery to all three examined sites was consistent with the fact that glutamatergic neurons in S1HL (S1HL^{Glu}) are responsible for encoding nociceptive information for the hindpaw^{21,35}. Together, these data

indicated that the somatosensory cortex (S2 and S1) is involved in the pain-induced analgesia.

To investigate whether the same group of neurons is activated in the S2 during pain at diverse sites induced analgesia, we captured S2 neurons activated during capsaicin injections into the right forepaw or the cheek by using *Fos^{TRAP2A14}* CFA mice and performed c-Fos immunohistochemistry staining in these mice to label S2 neurons activated during capsaicin injections into the left forepaw (Fig. 2h). We found

Fig. 2 | Increased neuronal activity in the S2 during pain-induced analgesia. **a** Schematic of TRAPing of the activated neurons in CFA mice following saline or CAP injection into the left forepaw, right forepaw, or cheek. **b–g** Quantification of TRAPed-tdTomato neuron expression in different brain regions with CAP or saline injected into the left forepaw (**b**, $n = 4$ slices from 4 mice; SIHL, $p = 0.0323$; SIFL, $p = 0.0089$; S2, $p = 0.0035$; Contra-S2, $p = 0.0495$), the right forepaw (**d**, $n = 4$ slices from 4 mice; SIHL, $p = 0.0016$; Contra-SIFL, $p < 0.0001$; S2, $p = 0.0010$; Contra-S2, $p < 0.0001$) and the cheek (**f**, $n = 4$ slices from 4 mice; SIHL, $p = 0.0319$; SIBF, $p = 0.0001$; S2, $p < 0.0001$; Contra-S2, $p < 0.0001$); representative images of tdTomato-positive neurons in S2 (**c**, **e**, **g**). Scale bar, 200 μm . **h** Schematic of TRAPing S2 neurons in CFA mice with CAP injection into the right forepaw or the cheek and employing c-Fos immunohistochemistry staining to label S2 neurons

activated by CAP injection in the left forepaw of the same mice. **i–l** Representative images (**i**, **k**) and overlap analysis (**j**, **l**) of the neural ensemble in the S2. The box indicates the magnified S2 region below. Scale bars, 200 μm (top) or 20 μm (bottom). Arrows indicate tdTomato-positive (red) or c-Fos-positive (brown) signals. L2–4, layer 2–4; ACC, anterior cingulate cortex; SIFL, primary somatosensory cortex of the forelimb area; Contra-SIFL, contralateral SIFL; SIBF, primary somatosensory cortex of the barrel field; Contra-S2, contralateral S2; IC, insular cortex; PVH, paraventricular hypothalamic nucleus; PAG, periaqueductal gray. Significance was assessed by two-way repeated-measures ANOVA with post hoc comparison in **b**, **d**, and **f**. All data are presented as the mean \pm SEM. * $P < 0.05$, ** $P < 0.01$, *** $P < 0.001$. Details of the statistical analyses are presented in Supplementary Data 2. Source data are provided as a Source Data file.

-70% overlap between S2 neurons activated by capsaicin injection in the left forepaw and in the right forepaw of CFA mice (Fig. 2i, j), as well as an -72% overlap of S2 neurons activated by capsaicin injection in the left forepaw and in the cheek of CFA mice (Fig. 2k, l).

To assess whether similar ensembles of neuronal activation in S2 are caused by noxious stimulation at diverse sites (i.e., rather than by neurons that are more active basally), we captured S2 neurons activated by saline injections into the right forepaw or the cheek by using *Fos^{TRAP2:Alu4}* CFA mice. Two weeks later, we performed c-Fos immunohistochemistry staining in these mice to label S2 neurons activated by capsaicin injections into the left forepaw (Supplementary Fig. 8a). We found -8% overlap of S2 neurons activated by saline injection in the right forepaw and capsaicin injection in the left forepaw of CFA mice (Supplementary Fig. 8b, c), as well as a -11% overlap of S2 neurons activated by saline injection in the cheek and capsaicin injection in the left forepaw of CFA mice (Supplementary Fig. 8d, e). Additionally, we captured S2 neurons activated by capsaicin injections into the right forepaw or into the cheek by using *Fos^{TRAP2:Alu4}* CFA mice; two weeks later, we performed c-Fos immunohistochemistry staining in these mice to label S2 neurons activated by saline injections into the left forepaw (Supplementary Fig. 8f). We found -9% overlap of S2 neurons activated by capsaicin injection in the right forepaw and saline injection in the left forepaw (Supplementary Fig. 8g, h), as well as a -8% overlap of S2 neurons activated by saline injection in the cheek and capsaicin injection in the left forepaw (Supplementary Fig. 8i, j). Taken together, these results suggested that distinct sites of noxious stimuli, rather than increased basal activity, produce similar ensembles of neuronal activation in S2. Based on this evidence, we subsequently administered capsaicin injections to the left forepaw of *Fos^{TRAP2}* mice to examine S2 neuronal activation during pain-induced analgesia, unless otherwise stated.

The S2 mediates pain-induced analgesia by inhibiting SIHL^{Glu} neuronal activity

Given the observed increase in c-Fos expression in the S2 and decrease in SIHL, we next investigated the potential roles of S2 and SIHL^{Glu} neurons in pain-induced analgesia. We simultaneously profiled the S2 and SIHL^{Glu} neuronal activity patterns by monitoring calcium response with microendoscopic imaging. Specifically, we infused an AAV expressing the Cre-dependent fluorescent Ca^{2+} indicator GCaMP6m (AAV-DIO-GCaMP6m) into the S2 and an AAV expressing the CaMKII-dependent fluorescent Ca^{2+} indicator GCaMP6m (AAV-CaMKII-GCaMP6m) into the SIHL of *Fos^{TRAP2}* mice, accompanied by mounting a microendoscopic gradient index (GRIN) lens mounted above the S2 and SIHL (Fig. 3a and Supplementary Fig. 9a–e). After injecting capsaicin or saline into the left forepaw, simultaneous monitoring of TRAPed S2 and SIHL^{Glu} neuronal activity revealed a significant increase in both Ca^{2+} transient frequency and mean z-scored activity of TRAPed S2 neurons in CFA mice with capsaicin injection in the left forepaw (Fig. 3b, c). In contrast, capsaicin injection to the left forepaw resulted in a significant decrease in both Ca^{2+} transient frequency and mean

z-scored activity of SIHL^{Glu} neurons (Fig. 3d, e). Thus, noxious stimulus delivery to the left forepaw results in activation of S2 neurons but inhibition of SIHL^{Glu} neurons in CFA mice (Supplementary Movie 5).

To examine whether the altered neuronal activity in S2 and SIHL was caused by the directed attention to a stimulus, we injected CQ into the left forepaw and simultaneously profiled S2 and SIHL^{Glu} neuronal activity patterns by monitoring calcium responses with microendoscopic imaging (Supplementary Fig. 9f). We observed no significant change in Ca^{2+} transient frequency or mean z-score activity in either TRAPed S2 or SIHL neurons during the CQ-evoked scratching period (Supplementary Fig. 9g–j). These results suggest that noxious stimuli, rather than attention to a stimulus, are required for the activation of S2 neurons and inhibition of SIHL^{Glu} neurons in pain-induced analgesia.

To connect the calcium response to the mouse's pain-related behaviors, we used microendoscopic imaging to record time-locked SIHL^{Glu} neuronal responses upon stimulation with a range of mechanical forces (0.07, 0.16, 0.4 and 0.6 g) in CFA mice with saline injected in the forepaw (Supplementary Fig. 10a, b). We found that both Ca^{2+} transient frequency and mean z-score of SIHL^{Glu} neuronal activity was significantly increased at suprathreshold stimuli of 0.16, 0.4, and 0.6 g (Supplementary Fig. 10c–j). We then injected CAP into the forepaw of the same mice and again recorded Ca^{2+} activity in SIHL^{Glu} neurons in response to different mechanical stimuli. Following CAP injection, we observed a lower increase in Ca^{2+} transient frequency and mean z-score of SIHL^{Glu} neuronal activity at 0.16, 0.4 and 0.6 g suprathreshold stimulation (Supplementary Fig. 10c–j). Taken together, these results suggested that delivery of the noxious stimuli to the forepaw led to inhibition of SIHL^{Glu} neurons in CFA mice.

We subsequently used a chemogenetic method to inhibit TRAPed S2 neurons wherein a Cre-dependent hM4Di-mCherry virus (AAV-DIO-hM4Di) was infused into the S2 of *Fos^{TRAP2}* mice and monitored SIHL^{Glu} neuronal activity by injecting an AAV-CaMKII-GCaMP6m virus into the SIHL with a GRIN lens implanted above (Fig. 3f). Briefly, inhibition of TRAPed S2 neurons abolished both the decrease in Ca^{2+} transient frequency and the decrease in mean z-scored activity of SIHL^{Glu} neurons in CFA mice with capsaicin injection in the left forepaw (Fig. 3g, h). Further, inhibition of S2 neurons blocked the pain-induced hindpaw analgesia; that is, CFA mice with capsaicin injection of left forepaw displayed no increase in nociceptive threshold of the left hindpaw (Fig. 3i, j). By contrast, we found that chemogenetic inhibition of TRAPed S2 neurons did not induce any significant decrease in nociceptive threshold in the hindpaw of naïve mice, suggesting that the observed pain-induced analgesia upon inhibition of TRAPed S2 neurons was paradigm-dependent (Supplementary Fig. 11a, b). Additionally, chemogenetic activation of TRAPed S2 neurons by infusion of a Cre-dependent hM3Dq-mCherry virus (AAV-DIO-hM3Dq) into S2 of *Fos^{TRAP2}* mice resulted in significantly increased nociceptive thresholds in CFA mice (Supplementary Fig. 11c, d). These results demonstrate that the S2 mediates pain at diverse sites induced analgesia, specifically by inhibiting the activity of SIHL^{Glu} neurons.

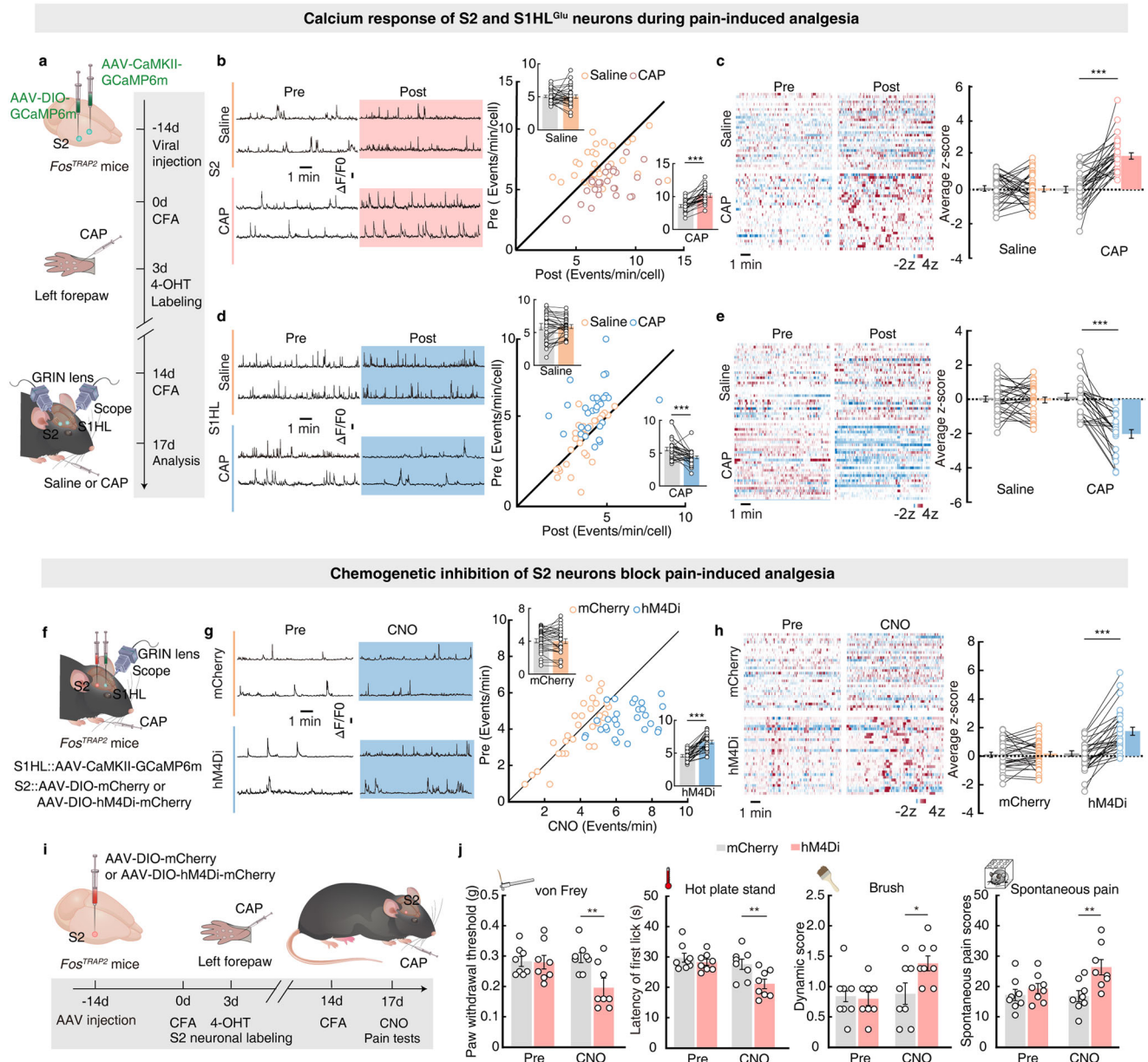


Fig. 3 | Activation of the S2 neuronal ensemble is required for pain-induced analgesia. **a** Schematic of simultaneous microendoscopic calcium imaging of S2 and SIHL^{Glu} neurons. **b–e** Representative traces (left) and summarized data (right) of spontaneous Ca²⁺ signals as well as heatmaps of the activities (left) and z-score responses (right) of TRAPed S2 neurons (**b**, $p < 0.0001$, **c**, $p < 0.0001$; $n = 30$ cells from 4 mice for Saline group; $n = 29$ cells from 3 mice for CAP group) and GCaMP6m⁺ SIHL^{Glu} neurons (**d**, $p = 0.0006$, **e**, $p < 0.0001$; $n = 30$ cells from 3 mice for Saline group; $n = 30$ cells from 3 mice for CAP group). **f** Schematic of microendoscopic calcium imaging of SIHL^{Glu} neurons. **g**, **h** Representative traces (left) and summarized data (right) of spontaneous Ca²⁺ signals as well as heatmaps of the activities (left) and z-score responses (right) of SIHL^{Glu} neurons before and during

inhibition of TRAPed S2 neurons (**g**, $p < 0.0001$, **h**, $p < 0.0001$; $n = 30$ cells from 3 mice for Saline group; $n = 29$ cells from 3 mice for CAP group). **i** Timeline of the chemogenetic inhibition of S2 neurons. **j** Effects of the inhibition of S2 neurons on nociceptive thresholds of the left hindpaw in CFA mice with CAP injection in the left forepaw ($n = 8$ mice per group; von Frey, $p = 0.0043$; Hot plate, $p = 0.0082$; Brush, $p = 0.0334$; Spontaneous pain, $p = 0.0043$). Significance was assessed by two-tailed paired Student's *t*-test in **b–h** and two-way repeated-measures ANOVA with post hoc comparison between groups in **j**. All data are presented as the mean \pm SEM. * $P < 0.05$, ** $P < 0.01$, *** $P < 0.001$. Details of the statistical analyses are presented in Supplementary Data 2. Source data are provided as a Source Data file.

An S2 \rightarrow SIHL feedforward inhibitory circuit controls pain-induced analgesia

To characterize connections between TRAPed S2 and SIHL^{Glu} neurons, we employed a cell type-specific anterograde trans-synaptic tracing system in which a Cre-dependent TK-GFP virus (AAV-DIO-TK-GFP) was injected into the S2 of *Fos*^{TRAP2} mice to facilitate the monosynaptic anterograde spread of an HSV- Δ TK-tdTomato virus injected at the same site three weeks later (Fig. 4a). After virus expression, we detected tdTomato⁺ signals in the primary

motor cortex, primary somatosensory cortex of the upper lip region, SIHL, SIFL, S1BF, contralateral S2, lateral globus pallidus (LGP), and ventral postero thalamic nucleus (VP) (Fig. 4b and Supplementary Fig. 12a, b). These tdTomato⁺ signals were primarily distributed in layer 4 of the SIHL, and co-localized with both a glutamate-specific antibody (~30%) and a GABA-specific antibody (~65%) (Fig. 4c). These results support a layer-specific organization wherein TRAPed S2 neurons predominantly innervate GABA neurons in layer 4 of SIHL.

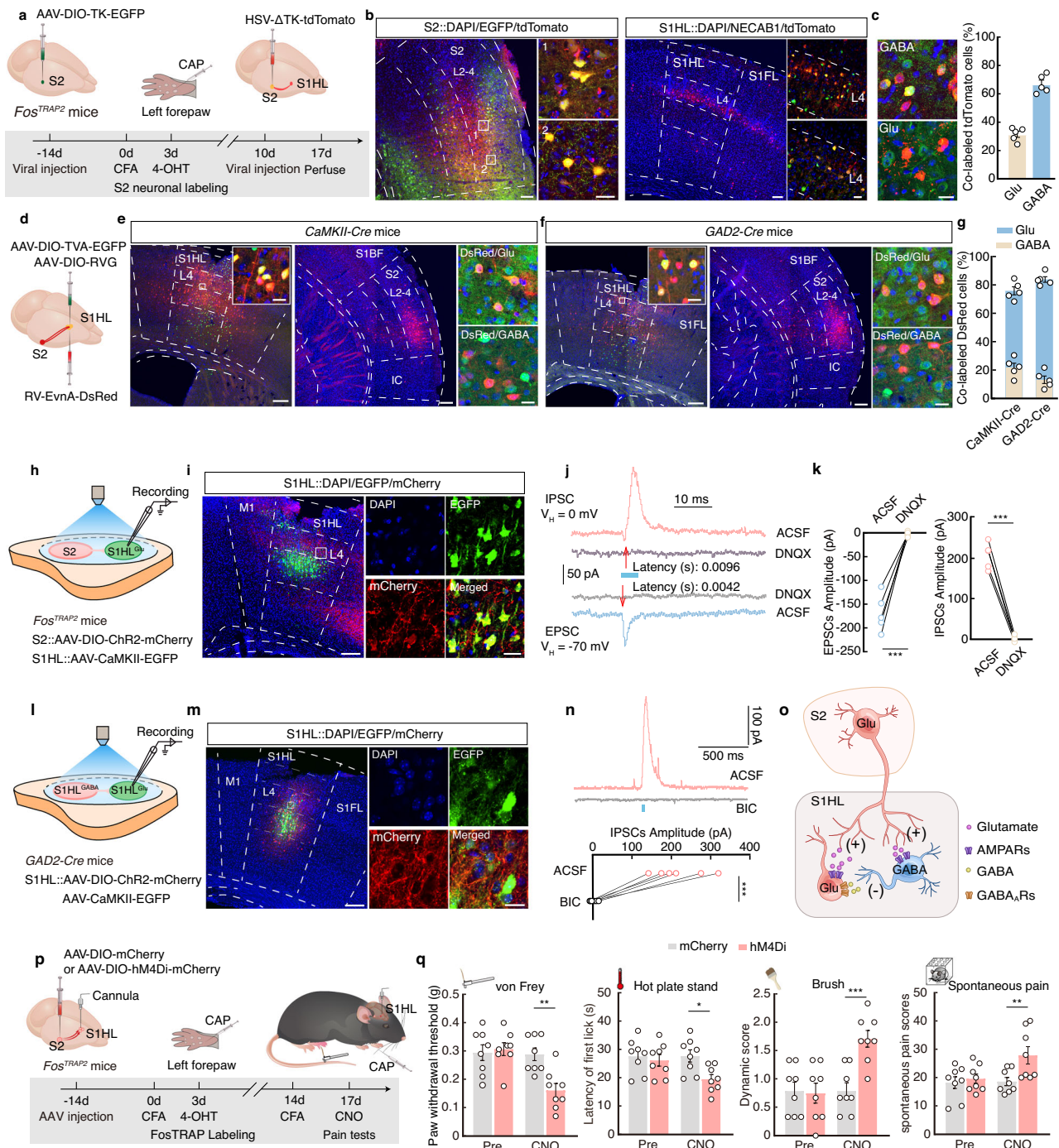


Fig. 4 | An S2 → SIHL^{GABA} → SIHL^{Glu} feedforward inhibitory circuit mediates ipsilateral pain-induced hindpaw analgesia. **a** Schematic of virus injection. **b** Representative images of the injection site (left) and tdTomato⁺ neurons in the SIHL that co-localized with NECAB1 antibody (right). The white box indicates the magnified S2 region in the inserts. Scale bars, 100 μm (left) or 20 μm (right). **c** Typical image (left) and summarized data (right) of tdTomato⁺ neurons in SIHL co-localized with glutamate and GABA immunofluorescence (*n* = 5 slices from 3 mice). **d** Schematic of virus injection. **e, f** Representative images of viral expression within the SIHL and DsRed⁺ neurons in the S2 co-localized with glutamate or GABA immunofluorescence of *CaMKII-Cre* mice (**e**) and *GAD2-Cre* mice (**f**). Scale bars, 200 μm or 20 μm. **g** Summarized data of DsRed expression in S2 predominantly co-localized with glutamatergic neurons (*n* = 5 slices from 3 mice per group). **h** Schematic of whole-cell recordings. **i** Representative images of viral expression within the SIHL. Scale bars, 100 μm (left) or 20 μm (right). **j, k** Representative traces

(**j**) and summarized data (**k**, left, *p* = 0.0009; right, *P* < 0.0001) recorded from the same SIHL^{Glu} neurons after photo-stimulation of S2 fibers. **l** Schematic of whole-cell recordings. **m** Representative images of the injection site within the SIHL. Scale bars, 100 μm (left) or 20 μm (right). **n** Representative traces of light-evoked currents (blue bar) before and after BIC treatment. **o** Schematic of an S2 → SIHL^{GABA} → SIHL^{Glu} circuit. **p** Timeline of chemogenetic inhibition of the TRAPed S2 → SIHL circuit. **q** Effects of inhibition of the S2 → SIHL circuit on nociceptive thresholds of the left hindpaw in CFA mice with CAP injection in the left forepaw (*n* = 8 mice per group; von Frey, *P* = 0.0020; Hot plate, *P* = 0.0152; Brush, *P* = 0.0005; Spontaneous pain, *P* = 0.0059). CAP, capsaicin; BIC, bicuculline. Significance was assessed by two-way repeated-measures ANOVA with post hoc comparison between groups in **q**, and two-tailed paired Student's *t*-test in **k** and **n**. All data are presented as the mean ± SEM. **P* < 0.05, ***P* < 0.01, ****P* < 0.001. Details of the statistical analyses are presented in Supplementary Data 2. Source data are provided as a Source Data file.

To characterize the detailed organization of this S2 to SIHL connection, we subsequently used a cell type-specific retrograde transmonosynaptic tracing strategy in which Cre-dependent helper viruses (AAV-EF1 α -DIO-TVA-GFP and AAV-EF1 α -DIO-RVG) were injected into the SIHL of *CaMKII-Cre* mice to facilitate spread of a monosynaptic retrograde rabies virus (RV) EnvA-pseudotyped RV- Δ G-DsRed injected at the same site three weeks later (Fig. 4d). We identified intensely DsRed-labeled neurons in the S2 that co-stained with glutamatergic neurons (Fig. 4e). Using a similar tracing strategy in *GABA synthetic enzyme glutamic acid decarboxylase 2 (GAD2)-Cre* mice, we again detected abundant DsRed signals in the S2 that co-stained with glutamatergic neurons (Fig. 4f, g). Thus, both SIHL^{Glu} and SIHL^{GABA} neurons receive direct innervation from the S2.

We next examined functional connections of the TRAPed S2 to SIHL circuit by infusing an AAV-DIO-ChR2-mCherry virus into the S2 and an AAV-CaMKII-GFP virus into the SIHL of *Fos^{TRAP2}* mice (Fig. 4h, i). We recorded light-evoked postsynaptic currents in SIHL^{Glu} neurons in voltage-clamp mode using an internal solution containing Cs-methanesulfonate and QX-314. At -70 mV holding potential, photostimulation of ChR2-expressing TRAPed S2 terminals in SIHL evoked reliable excitatory postsynaptic currents (EPSCs) from SIHL^{Glu} neurons (Supplementary Fig. 12c, d). These EPSCs could be blocked by the AMPA receptor antagonist, 6,7-dinitroquinoxaline-2,3-dione (DNQX) (Fig. 4j, k). Except for these light-evoked EPSCs, at 0 mV holding potential, photo-stimulation also elicited IPSCs in the same neurons, which were also blocked by DNQX treatment (Fig. 4j, k). Notably, the latency to light-evoked IPSCs (latency: 0.0096 ms) was longer than that for EPSCs (latency: 0.0042 ms). These results suggested that SIHL^{Glu} neurons are innervated by local SIHL^{GABA} interneurons, both of which receive direct S2 inputs.

In addition, we found that upon AAV-DIO-ChR2-mCherry and AAV-CaMKII-EYFP injection into the SIHL of *GAD2-Cre* mice (Fig. 4l, m), blue light stimulation of local SIHL^{GABA} neurons resulted in significantly increased IPSCs in the SIHL^{Glu} (Supplementary Fig. 12e, f). These increased IPSCs were blocked by treatment with the GABA_A receptor antagonist, bicuculline (Fig. 4n), indicating that the SIHL^{GABA} neurons generated direct inhibitory projections to SIHL^{Glu} neurons. Together, these results identified a functional S2 \rightarrow SIHL^{GABA} \rightarrow SIHL^{Glu} feedforward inhibitory circuit (Fig. 4o). We then selectively monitor layer 4 of SIHL^{GABA} neuronal responses to capsaicin injection in the left forepaw of CFA mice by infusing AAV-DIO-GCaMP6m into the SIHL and mounting a GRIN lens at the top of the SIHL of *GAD2-Cre* mice (Supplementary Fig. 13a, b). Upon left forepaw injection with capsaicin, Ca²⁺ transient frequency and mean z-scored activity of these SIHL^{GABA} neurons increased (Supplementary Fig. 13c, d), suggesting that SIHL^{GABA} neurons are activated by noxious stimuli in the forepaw of CFA mice.

To determine whether the S2 \rightarrow SIHL^{GABA} \rightarrow SIHL^{Glu} circuit is required for pain-induced analgesia, we conducted chemogenetic inhibition experiments by infusing an AAV-DIO-hM4Di-mCherry or AAV-DIO-mCherry virus into the S2 and implanted a cannula in the SIHL of *Fos^{TRAP2}* mice (Fig. 4p). Three weeks following hM4Di expression, mice received an intracranial microinjection of the DREADD agonist CNO, with monitoring of the nociceptive threshold of the hindpaw. We found that any increase in hindpaw nociceptive thresholds was abolished upon chemogenetic silencing of the S2-S1 circuit (Fig. 4q). Additionally, S2 innervates inhibitory neurons in S1 is suggested to be involved in the planning of motor behavior³⁶. To determine whether the decreased nociceptive thresholds in the hindpaw observed upon inhibiting TRAPed S2 \rightarrow SIHL circuit was attributed to defects in motor responses, we performed motor behavior assays including the rotarod and paw angle test in *Fos^{TRAP2}* mice with intracranial microinjection of the CNO. We found that mice with a selectively silenced TRAPed S2 \rightarrow SIHL circuit showed no significant impairment in rotarod tests nor abnormal hindpaw angles compared

to control animals (Supplementary Fig. 14), indicating that silencing of the TRAPed S2 \rightarrow SIHL circuit does not induce motor response defects. Collectively, these results indicated that noxious stimuli in the left forepaw activate the S2 \rightarrow SIHL^{GABA} \rightarrow SIHL^{Glu} feedforward inhibitory circuit to mediate pain-induced analgesia without impairing locomotor function.

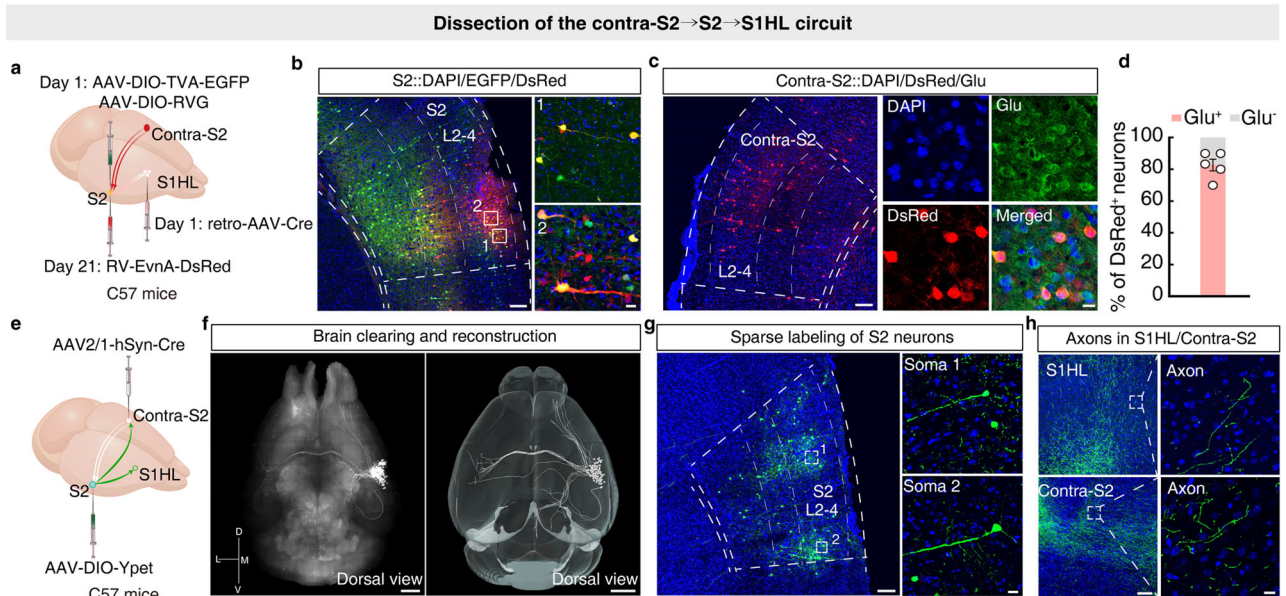
A contra-S2 \rightarrow S2 \rightarrow SIHL circuit mediates contralateral pain-induced analgesia

Previous studies have shown lateralization is a hallmark of somatosensory processing in the mammalian brain³⁷. Recalling that noxious stimuli delivered to the right forepaw (contralateral body part) inhibit pain-related behavior in the left hindpaw, whereas nociceptive information from the right body part is encoded by contralateral hemispheres^{27,38}. It is thus possible that contralateral S2 (contra-S2) innervation of the S2 \rightarrow SIHL circuit mediates analgesia of the left hindpaw induced by noxious stimuli in the right forepaw of CFA mice. To examine this possibility, we first sought to identify direct synaptic connections between the contra-S2 and S2 \rightarrow SIHL circuit using a triple retrograde tracing strategy in which retro-AAV-hSyn-Cre was injected into the SIHL of C57 mice, while Cre-dependent helper viruses were injected into the S2. After 3 weeks, RV- Δ G-DsRed was injected into the S2 (Fig. 5a, b). We detected DsRed⁺ signals in the secondary motor cortex, IC, lateral posterior thalamic nucleus, central medial thalamic nucleus, VP, LGP, basolateral amygdaloid nucleus and contra-S2 (which co-localized with glutamate antibody) (Fig. 5c, d and Supplementary Fig. 15a, b). These results thus demonstrated that the S2 \rightarrow SIHL circuit receives direct innervations from the contra-S2.

To help visualize the connectivity of this contra-S2 \rightarrow S2 \rightarrow SIHL circuit, we used sparse labeling of S2 neurons innervated by the contralateral S2 by injecting AAV-hSyn-Cre virus into the contra-S2 and AAV-DIO-YPet virus into the S2 of C57 mice (Fig. 5e). Three weeks after injection, we employed the CLARITY approach³⁹ to render the brain largely translucent, thus enabling whole-brain imaging of YPet⁺ fibers originating from S2 neurons. We found that the S2 displayed significant connections to contralateral S2, as well as ipsilateral projections to S1, and to the ipsilateral primary motor cortex (M1). The S2 also had substantial subcortical projections, the densest of which were observed in ventrolateral posterolateral thalamic nucleus (VPL), posterior complexes (Po), and lateral globus pallidus (LGP) of the thalamus. Other subcortical projections targeted the pontine reticular nucleus (PnO) and commissural stria terminalis (cst) (Fig. 5f-h and Supplementary Fig. 15c-e). These results collectively suggested that S2 neurons interact with contralateral S2 and also innervate the SIHL. To examine the functional connections of the contra-S2 \rightarrow S2 \rightarrow SIHL circuit, we injected an AAV-DIO-ChR2-mCherry into the contra-S2, and a retro-AAV-hSyn-EGFP into the SIHL of *Fos^{TRAP2}* mice (Supplementary Fig. 16a). Photo-stimulation of contra-S2 fibers elicited EPSCs in EGFP⁺ neurons of the S2, which were blocked by exposure to DNQX (Supplementary Fig. 16b, c). Together, these data thus illustrated a direct functional connection in the contra-S2 \rightarrow S2 \rightarrow SIHL circuit.

Subsequently, we examined neuronal activity in contra-S2, S2 and SIHL^{Glu} during contralateral pain-induced analgesia by monitoring calcium response with microendoscope imaging. For this experiment, an AAV-DIO-GCaMP6m was infused into the contra-S2 and S2, while AAV-CaMKII-GCaMP6m was infused in the SIHL of *Fos^{TRAP2}* mice, with GRIN lenses mounted above all three of these regions (Fig. 5i). Upon capsaicin injection to the right forepaw, we observed that Ca²⁺ transient frequency and mean z-scored activity both significantly increased in contra-S2 and S2 neurons (Fig. 5j-m). By contrast, both Ca²⁺ transient frequency and mean z-scored activity significantly decreased in SIHL^{Glu} neurons (Fig. 5n, o and Supplementary Movie 6).

We further chemogenetic inhibit contra-S2 neurons and monitored S2 and SIHL^{Glu} neuronal activity by injecting an AAV-DIO-GCaMP6m and AAV-CaMKII-GCaMP6m virus into the S2 and SIHL,



Calcium response of Contra-S2, S2 and S1HL^{Glu} neurons during contralateral pain-induced analgesia

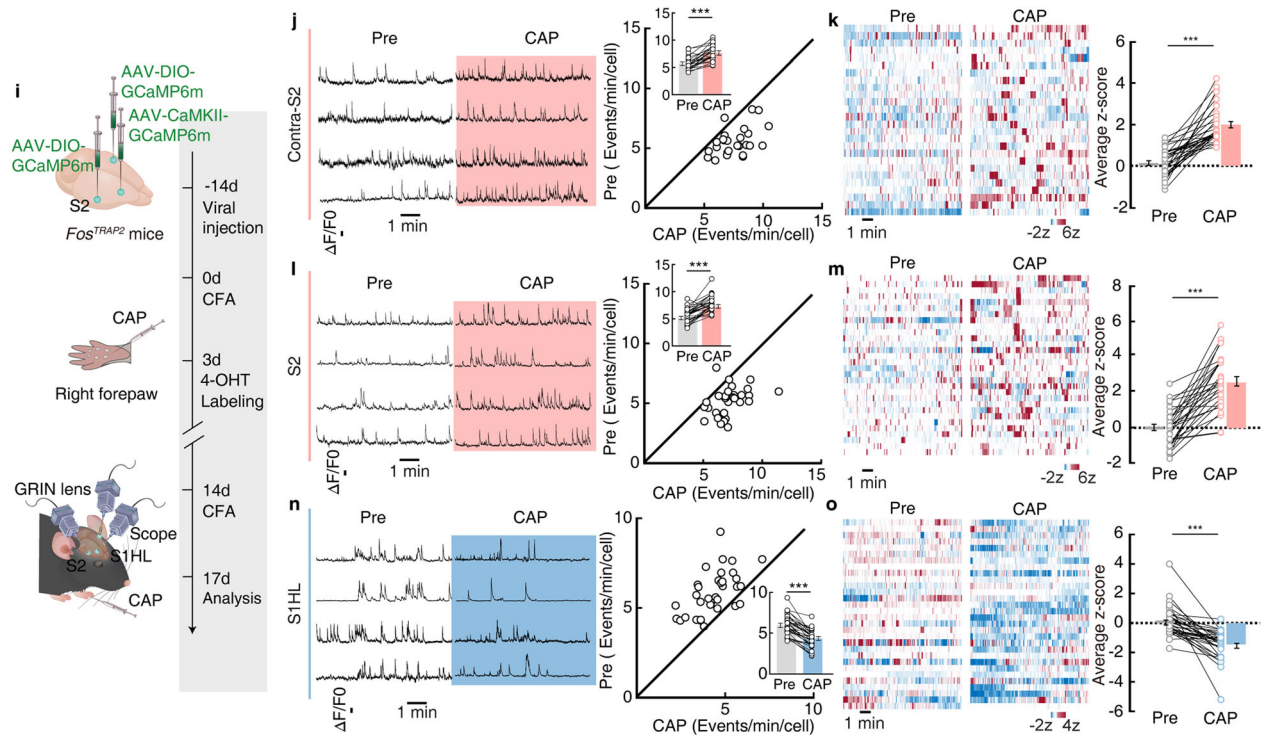


Fig. 5 | Activation of a contra-S2 → S2 → S1HL circuit during contralateral pain-induced hindpaw analgesia. **a** Schematic of the triple retrograde tracing strategy. **b** Representative images of the starter neurons (yellow) within the S2. Scale bars, 100 μ m. The white box represents the magnified S2 area in the inserts. Scale bar, 20 μ m. **c, d** Representative image (c) and summarized data (d; $n = 5$ slices from 3 mice) of RV-DsRed expression in contra-S2 predominantly co-localized with glutamate immunofluorescence. Scale bars, 100 μ m (left) or 10 μ m (right). **e** Schematic of the sparse labeling strategy. **f** Dorsal view of the reconstruction of S2 projection sites (left) and the 3D reconstruction of S2 projectome (right). Scale bars, 1 mm. **g** Fluorescence images of a S2 section expressing Ypet sparsely in soma. Scale bars, 100 μ m (left) or 20 μ m (right). **h** Fluorescence images of an S1HL (top) and contra-S2 (bottom) section expressing Ypet in S2 neuronal axon. Scale bars, 100 μ m (left) or

20 μ m (right). **i** Schematic of viral injections and simultaneous microendoscopic calcium imaging of contra-S2, S2, and S1HL^{Glu} neurons by CAP injection in the right forepaw. **j–o** Representative traces (left) and summarized data (right) of spontaneous Ca²⁺ signals as well as heatmaps of the activities (left) and z-score responses (right) of contra-S2 neurons (**j**, $p < 0.0001$, **k**, $p < 0.0001$, $n = 33$ cells from 4 mice), S2 neurons (**l**, $p < 0.0001$, **m**, $p < 0.0001$; $n = 32$ cells from 4 mice) and GCaMP6m⁺ S1HL^{Glu} neurons (**n**, $p < 0.0001$, **o**, $p < 0.0001$; $n = 34$ cells from 3 mice). CAP, capsaicin. Significance was assessed by two-tailed paired Student's *t*-test in **j–n** and Wilcoxon matched-pairs signed rank test in **o**. Data are presented as means \pm SEM. *** $p < 0.001$. Details of the statistical analyses are provided in Supplementary Data 2. Source data are provided as a Source Data file.

respectively (Fig. 6a). Inhibition of contra-S2 neurons blocked both increased S2 neuronal activity and decreased SIHL^{Glu} neuronal activity induced by capsaicin injection of the right forepaw in CFA *Fos^{TRAP2}* mice (Fig. 6b–e and Supplementary Movie 7). These results thus demonstrated the activation of a contra-S2 → S2 → SIHL circuit during contralateral pain-induced analgesia.

Finally, we examined whether the contra-S2 → S2 → SIHL circuit is essential for contralateral pain-induced analgesia by injecting AAV-DIO-hm4Di-mCherry or AAV-DIO-mCherry into the contra-S2 of *Fos^{TRAP2}* mice and implanting a cannula in the S2. Three weeks following hm4Di expression, mice received an intracranial microinjection of the CNO, with monitoring of the nociceptive threshold of the hindpaw. We found that increase in hindpaw nociceptive thresholds was abolished upon chemogenetic inhibition of the contra-S2 terminals in the S2 (Fig. 6f, g). These results cumulatively demonstrated that the observed ipsilateral pain-induced analgesia is mediated by the S2 → SIHL circuit and contralateral pain-induced analgesia is mediated by the contra-S2 → S2 → SIHL circuit (Supplementary Fig. 17).

Discussion

Here, we found that a neuronal ensemble in layers 2–4 of the bilateral secondary somatosensory cortex (S2) responds to noxious stimuli signals from diverse body regions. The S2 mediates ipsilateral pain-induced analgesia via feedforward inhibitory innervation of SIHL,

whereas contralateral S2 innervation of the S2 → S1 circuit mediates contralateral pain-induced analgesia.

S2, as a higher-order brain region for sensory integration, is involved in the processing and interpretation of pain signals, modulating pain through its downstream projections^{40,41}. Our study has identified the intra-somatosensory cortical circuits that underlie pain-induced analgesia. Specifically, noxious stimuli from the ipsilateral forepaw activates S2 → S1 circuit to mediate ipsilateral pain-induced hindpaw analgesia. Given the high degree of lateralization known for mammalian sensory and motor systems, noxious stimuli from contralateral forepaw activate the contralateral S2 which, through inter-hemispheric communication with the S2-S1 circuit, mediates contralateral pain-induced hindpaw analgesia. This connection between S2 and S1 is necessary for coordinating the perception of pain at diverse body regions and for the effect of contralateral noxious stimuli on pain modulation.

Superficial layers of the cortex are more involved in pain sensitization, the emotional and cognitive components of pain^{19,42,43}, whereas deeper layers directly modulate the sensory components of pain via downstream pathways^{21,24}. Recent studies have explored the specific role of different layers of S2 in pain modulation. Excitatory projection neurons, largely originating from layer 5a of S2, innervate M2 and govern mechanical and heat sensitivity, inhibition of S2-to-M2 projecting neurons enhances sensitivity⁴¹. By contrast, layer 6 of

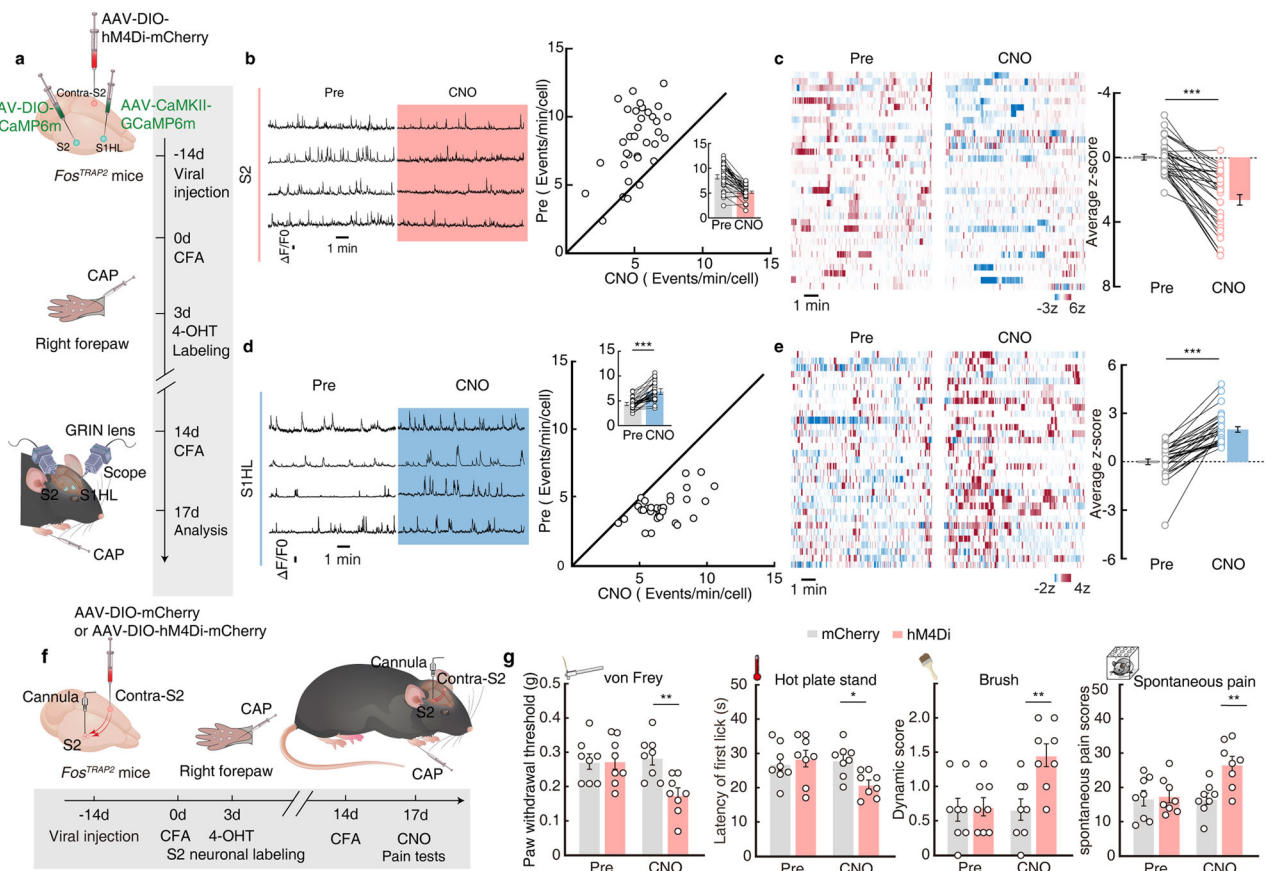


Fig. 6 | Contralateral S2 → S2 → SIHL circuit mediates contralateral pain-induced hindpaw analgesia. **a** Schematic of simultaneous microendoscopic calcium imaging of S2 and SIHL^{Glu} neurons after optogenetic inhibition of TRAPed contra-S2 neurons. **b–e** Representative traces (left) and summarized data (right) of spontaneous Ca²⁺ signals as well as the heatmaps of the activities (left) and z-score responses (right) of GCaMP6m⁺ S2 neurons (**b**, $p < 0.0001$, **c**, $p < 0.0001$; $n = 34$ cells from 4 mice) and GCaMP6m⁺ SIHL^{Glu} neurons (**d**, $p < 0.0001$, **e**, $p < 0.0001$; $n = 24$ cells from 4 mice) after inhibition of TRAPed contra-S2 neurons. **f** Timeline of chemogenetic inhibition of the contra-S2 → S2 → SIHL circuit in CFA mice with CAP

injection in the right forepaw. **g** Effects of chemogenetic inhibition of contra-S2 → S2 → SIHL circuit on the nociceptive threshold of the left hindpaw in CFA mice with CAP injection in the right forepaw ($n = 8$ mice per group; von Frey, $p = 0.0033$; Hot plate, $p = 0.0262$; Brush, $p = 0.0024$; Spontaneous pain, $p = 0.0032$). CAP, capsaicin. Significance was assessed by two-way repeated-measures ANOVA with post hoc comparison between groups in **g**, two-tailed paired Student's *t*-test in **b–d**, and Wilcoxon matched-pairs signed rank test in **e**. Data are presented as means ± SEM. * $P < 0.05$; ** $P < 0.01$; *** $P < 0.001$. Details of the statistical analyses are provided in Supplementary Data 2. Source data are provided as a Source Data file.

glutamatergic neurons in S2 was inhibited by noxious stimulation, and optical inhibition and activation of projection terminals of layer 6 of S2^{Glu} in the VPL and Po reduced and enhanced bilateral nociceptive sensitivity, respectively⁴⁰. Using a pain-induced analgesia paradigm, our study showed that neurons in layers 2–4 of S2 were activated in response to noxious stimuli. These neurons mediate pain-induced analgesia through projections specifically to layer 4 of SIHL. These cumulative studies collectively reveal functional heterogeneity among neurons across different layers of S2 in pain modulation by projecting to different downstream brain regions.

Moreover, S2 projections to S1 have been shown to preferentially innervate PV⁺ and SST⁺ inhibitory neurons to regulate motor function (e.g., rotarod and paw angle tests)³⁶. Tests of motor-related behaviors in CFA-hindpaw mice with chemogenetic silencing of TRAPed S2 neurons showed no significant impairment of motor responses in these animals. It should be noted that only limited subset of S2 neurons that are activated under pain-induced analgesia and specifically project to SIHL were silenced in our experiments, which may not be sufficient to induce a deficit in motor function. These studies reveal that the possible existence of distinct populations of S2 neurons that regulate pain sensation and motor function, respectively.

Lateralization, wherein information from one body side is primarily processed in the contralateral hemisphere, is a hallmark of somatosensory processing^{44,45}. Ascending sensory information is projected to contralateral brain regions through spinal projection neurons, with the contralateral thalamus as the primary projection target; this spinothalamic pathway is known to convey pain, itch, touch, and temperature information to the contralateral cortex^{31,38,46}. Consistent with this notion, our study indicates that S2 activation is mediated by contralateral S2 (contra-S2) innervation in CFA mice given capsaicin injection of the right forepaw. Our findings, together with another recent study that showed unilateral tactile stimulation can modulate S2 neuronal activity in both cerebral hemispheres by corticocortical projections via the corpus callosum⁴⁴, suggest that interhemispheric communication is essential for unilateral somatosensory stimulation to elicit a bilateral S2 response.

In mice, we found that pain-induced analgesia effect varies with the intensity of the stimulus. Our results showed that a 1 µg/10 µl concentration of capsaicin injected in the forepaw did not significantly increase the nociceptive threshold in inflamed hind paws of CFA mice, whereas both 5 µg/10 µl and 10 µg/10 µl concentrations injected in the forepaw significantly increased the nociceptive threshold, and we observed prominent increases in the nociceptive threshold of the CFA mice at the higher capsaicin concentration.

It is worth noting that the decrease in sensitivity and changes neuronal activity induced by noxious stimuli are unlikely due to attention distraction, as we found that injection of with the pruritogen agent chloroquine into the forepaw of mice induced significant scratching behavior but did not alter the nociceptive thresholds of the inflamed hindpaw or the neuronal activity of TRAPed S2 or SIHL neurons. Thus, the “pain-inhibiting pain” phenomenon is unlikely to result from an attentional change. Additionally, previous studies of humans^{1,2,47} have examined whether distraction and pain stimulation inhibit pain through the same or different mechanisms, specifically by looking at whether there is a similar or even an additive effect on pain attenuation. Briefly, these studies found that the effects of pain and distraction are independent, and that the “pain-inhibiting pain” phenomenon cannot be attributed solely to distraction, but rather require a pain stimulus.

Taken together, our findings define layer-specific intra-somatosensory cortical circuits that mediates pain-induced analgesia. These findings enrich our understanding of somatosensory cortex function and also highlight the functional heterogeneity among neurons across different layers of the S2 in pain sensation. Examining how this circuit works in collaboration with other defined descending projections from

the brainstem to the spinal cord in DNIC is likely to be a fruitful area for future investigations.

Methods

Animals

All experiments were approved by the University of Science and Technology of China (USTC). Animals utilized in the procedures were obtained from Charles River or Jackson Laboratories and were bred at the animal facility at USTC. These included C57BL/6J, *Ail4* (RCL-tdT), *Fos*^{TRAP2}, *CaMKII-Cre* and *GAD2-Cre* male mice aged 8–10 weeks. Mice were randomly assigned to groups of five individuals per cage randomly, except in cases where a GRIN lens was implanted. A stable environment was maintained with a temperature range of 23–25 °C and a 12-hour light/dark cycle (lights on from 7:00 a.m. to 7:00 p.m.). Mice had *ad libitum* access to water and food. Certain mice were excluded from further analyses due to missed targets in viral tracing, *in vivo* recording, and behavioral data collection, such as failed virus injections or incorrect optic fiber and GRIN lens placement.

Mouse models

Complete Freund's adjuvant injection. Inflammatory pain was induced by injecting complete Freund's adjuvant (CFA, 10 µl, Sigma) into the plantar of the left hindpaw of each mouse under brief isoflurane anesthesia.

Pinch stimulus application. A noxious pinch stimulus was applied to the skin surface of the left forepaw, right forepaw, and cheek using an alligator clip (Generic Micro Steel10 Alligator Test Clips), as previously described⁴⁸. For control mice, alligator clips were taped to the skin surface of the corresponding body site. For the cheek pinch, we selected a location about 2 cm from the ear (towards the nose), an area where facial muscles are abundant. The clip was gently applied to the muscle.

Capsaicin injection. Capsaicin (Sigma, M2028) was dissolved in alcohol at a concentration of 100 mg/ml and then diluted to a 1 mg/ml working solution with saline. Subsequently, 10 µl of capsaicin was subcutaneously injected into the left forepaw, right forepaw and cheek of mice to induce tonic pain. Control mice received an injection of the same quantity of saline (0.9% NaCl). Mice subjected to CAP injection were not used to test other pain-induced analgesia models in behavioral tests.

Behavior tests

von Frey test. von Frey test was conducted to assess mechanical pain threshold in mice. Prior to the experiments, mice were individually placed in clear plastic chambers on a wire mesh grid for 30 minutes per day for 3 days to habituate them to the environment. For the test, a series of von Frey filaments with ascending forces ranging from 0.02 to 1g were used. These filaments were perpendicularly applied to the plantar surface of the left hindpaw with sufficient force to bend them. The withdrawal threshold was calculated as the average of five applications of the minimal filament force when the mice either withdrew their paw or licked it.

Dynamic tactile allodynia. Dynamic tactile allodynia was assessed following the same preparatory procedure as the von Frey filament test. The method used for measuring dynamic tactile allodynia was consistent with previous reports⁴⁹. In brief, a 5/0 brush was gently stroked along the left hindpaw from heel to toe at a speed of approximately 2 cm/s. The response was scored as follows: 0 = no response; 1 = very quick slight movement or lifting of the paw; 2 = sustained lifting of the paw for more than 2 seconds towards the body or strong lateral lifting above the body level; and 3 = flinching multiple times or licking the paw, excluding grooming behavior. Three

successful tests were performed for each mouse at intervals of more than 5 minutes to obtain a mean score.

Hot plate test. Hot plate test was conducted in accordance with previously established protocols⁵⁰. Mice were positioned on a 52 °C hot plate enclosed by four Plexiglas walls and a lid to prevent escape. The latency to the first instance of licking the left hindpaw was recorded.

Spontaneous pain. To assess spontaneous pain, individual mice were placed in transparent chambers with wire grid floors and recorded via video for 30 minutes. Subsequently, the video footage was played back in slow motion, and occurrences of licking and flinching, shaking, or lifting events involving the hindpaw were manually tallied. Movements associated with locomotion, body repositioning, and grooming were excluded from the count. Each bout of licking was scored as 2 points, while each bout of flinching, shaking, or lifting was scored as 1 point. The cumulative points obtained over the 30-minute recording period constituted the spontaneous pain score⁵¹.

Rotarod assay. We evaluated motor response and coordination through accelerating rotarod tests^{36,52}. Each mouse was tested in two sessions, with three rotarod trials per session and a 3 h recovery interval between sessions, so that each mouse underwent six total trials per day. In the trial, individual mice were positioned on the rotarod and rotation speed accelerated from 0 to 40.2 rpm over a 300 s test period. Researchers recorded the duration each mouse spent on the rotarod. Mice were allowed 5 min recovery periods prior to each trial. The trial was halted when the mouse failed to maintain balance, defined as clinging to the rod for three consecutive rotations or falling off the rotarod altogether.

Locomotion assays. To assess changes or impairment in locomotion of the mice, we acquired gait image data of the hindpaw angles using a DigiGait™ Imaging System (Mouse Specifics, Inc., USA). Prior to gait analysis, mice were trained to walk on a transparent treadmill for 5 min, once per day, over a three-day period. After completing the training period, mice were positioned on the treadmill and the running behavior of each mouse was recorded with the above imaging system. Statistical analyses were conducted on imaging data obtained in a 2 s interval of uniform running speed using the DigiGait Analyses software.

Itch behavior test. Mice were individually placed in a clear plastic chamber for at least 1 hour on 2 consecutive days for acclimatization. On the day of the behavioral test, the mice were again acclimated to the test chamber for 30 min. After intradermal injection of chloroquine (100 µg/10 µl, C6628, Sigma) into the cheek, scratching behaviors were recorded on video for 30 min. One bout of scratching was defined as an episode in which a mouse lifted its hindpaw and scratched for any length of time until the paw was placed back to the ground or to the mouth. After intradermal injection of chloroquine into the forepaw, a digital video camera was used to record the itch-induced biting behavior. One bout of biting was defined as an episode in which a mouse lifted its forepaw and bit the injection site continuously until the paw was leave mouth^{53,54}. Slow-motion playback of the video was used to quantification of the number of scratching or biting bouts.

Activity-dependent cell labeling

To achieve activity-dependent labeling of neurons during pain-induced analgesia, we habituated all mice daily for at least 3 days to ensure full adaptation to the test room before TRAP labeling. Subsequently, the mice received an intraperitoneal (i.p.) injection of 4-Hydroxytamoxifen (4-OHT, 50 mg/kg in corn oil; Sigma-Aldrich), followed by an injection of 10 µl capsaicin into either the left forepaw,

right forepaw, or cheek, 30 minutes later. For enabling Cre-dependent viral expression in active S2 or contralateral S2 neurons, *Fos*^{TRAP2} mice received an intraperitoneal injection of 4-OHT two weeks after viral injection, preceding capsaicin administration into the forepaw. Following two weeks of viral expression, the mice were prepared for further experiments.

Stereotaxic surgeries and viral injections

After administering an intraperitoneal injection of pentobarbital (20 mg/kg), mice were anesthetized, with a heating pad used to maintain body temperature. Following this, the hair was shaved, and the head was securely fixed in a stereotaxic device (RWD, Shenzhen, China). The scalp was then incised to expose the skull, and adjustments were made to ensure proper skull alignment in all planes.

Subsequently, with the injection site visible under the stereoscope, the skull was perforated using a hand drill. Virus injection followed, employing a syringe fitted with a pulled glass microelectrode and connected infusion pump (micro 4, WPI). A volume of 100–300 nl virus was injected into the target area at a rate of 35 nl/min. Throughout the injection process, the pipette remained at the injection site for 5 minutes to prevent virus diffusion.

For anterograde trans-monosynaptic tracing, we injected rAAV-Eflα-DIO-EGFP-T2A-TK-WPRE-hGHpA (AAV-DIO-TK, AAV2/9, 5.66E × 10¹² vg ml⁻¹, 200 nl, *BrainVTA*) into the S2 at coordinates of ML (medial-lateral) -4.20 mm, AP (anterior-posterior) -0.95 mm, DV (dorsal-ventral) -1.55 mm from bregma. One week following 4-OHT injection, HSV-ΔTK-LSL-tdTomato (HSV-ΔTK-tdTomato, 1.00E + 09 PFU/mL, 200 nl, *BrainVTA*) was injected into the same location of the S2. After allowing 7 days for viral expression, the mice were perfused, and their brains were cryosectioned to examine the tdTomato signals originating from the S2 neurons. For the sparse labeling strategy, AAV2/1-hSyn-Cre-WPRE-pA (AAV-hSyn-Cre, 2.1E × 10¹³ vg ml⁻¹, 180 nl, *BrainVTA*) was injected into the contralateral S2, while rAAV-EFlα-DIO-Ypet-2A-mGFP-WPRE-pA (AAV-DIO-Ypet, 5.18 E × 10¹² vg ml⁻¹, diluted 1:1000, 180 nl, *BrainVTA*) was injected into the S2.

For retrograde trans-monosynaptic RV tracing, we unilaterally injected a helper virus containing rAAV-Eflα-DIO-RVG-WPRE-pA (AAV-DIO-RVG, AAV2/9, 2 × 10¹² vg ml⁻¹) and rAAV-EFlα-DIO-EGFP-T2A-TVA (AAV-DIO-EGFP, AAV2/9, 2 × 10¹² vg ml⁻¹; 1:1, 200 nl, Brain Case) into the SIHL (ML -1.6 mm, AP -0.48 mm, DV -4.3 mm) of *CaMKII-cre* mice or *GAD2-cre* mice. Three weeks later, RV-EnvA-ΔG-DsRed (2 × 10⁸ IFU ml⁻¹, 300 nl) was injected into the SIHL using identical conditions and coordinates. Seven days after the last injection, we perfused the mice and prepared brain slices for tracing the DsRed signal or performing immunohistochemistry with glutamate-specific or GABA-specific antibodies. For triple tracing, we injected retro-AAV-hSyn-Cre-WPRE (retro-AAV-hSyn-Cre, 200 nl, *BrainVTA*) into the SIHL of C57BL/6J mice, and infused the Cre-dependent mixed helper virus into the ipsilateral S2. Three weeks later, we injected RV-DsRed into the same location of the S2. After 10 days, we prepared brain slices for tracing the DsRed signal.

For optogenetic manipulation, we delivered the Cre-dependent virus rAAV-Eflα-DIO-hChR2 (H134R)-mCherry-WPRE-pA (AAV-DIO-ChR2-mCherry, AAV2/9, 1.63 × 10¹³ vg/ml, 200 nl, *BrainVTA*) into the S2 of *Fos*^{TRAP2} mice or the SIHL of *GAD2-cre* mice. After three weeks, we detected the expression of mCherry throughout the whole brain. For chemogenetic manipulation, we used the rAAV-Eflα-DIO-hM4D(Gi)-mCherry-WPRE-pA (AAV-DIO-hM4Di-mCherry, AAV2/9, 3.69 × 10¹³ vg/ml, *BrainVTA*) viruses and implantation of the cannula in the downstream brain region. After viral expression, we administered CNO (1 mg/kg, Sigma-Aldrich, USA) intraperitoneally or delivered CNO (3 µM) by the implanted cannula, followed by pain-related behavior tests. The rAAV-Eflα-DIO-mCherry-WPRE-pA (AAV-DIO-mCherry, AAV2/8, 8.93 × 10¹² vg/ml, *BrainVTA*) virus served as the control.

For *in vivo* single-cell Ca^{2+} imaging, we injected the Cre-dependent AAV-DIO-GCaMP6m virus (1.0×10^{13} vg mL^{-1} , 200 nl, Brain Case) into the contralateral S2 and S2, and introduced the CaMKII-dependent fluorescent Ca^{2+} indicator GCaMP6m (AAV-CaMKII-GCaMP6m) into the SIHL of *Fos^{TRAP2}* mice. To simultaneously profile the calcium signals of S2 and SIHL^{Glu} neuronal activity during pain-induced analgesia, we utilized an integrated microendoscopic GRIN lens (0.5 mm in diameter \times 4 mm in length, Inscopix). The lens was tilted 20° to the left and slowly lowered (100 $\mu\text{m}/\text{min}$) towards SIHL, and then tilted 20° to the right and slowly lowered towards S2, ensuring that two lenses were implanted in a single mouse.

To achieve the correct spatial arrangement of simultaneously implanted lenses in bilateral S2 and S1 within a single mouse, we positioned the lenses at a 20° -degree tilt using the following detailed steps: After virus injection, we used a stereotaxic device (RWD, Shenzhen, China) to tilt the baseplate of a 7.3 mm lens by 20° to the lateral side (left) for implantation in the left hemisphere of S2. After fixation with tissue glue and dental cement, we tilted the baseplate of a 4.0 mm lenses to the right by 20° for implantation into the right hemisphere of S2, and fixed this baseplate to the skull with tissue glue and dental cement. Finally, we tilted the baseplate of a 7.3 mm lens 20° to the left for implantation into the right hemisphere of the SIHL.

All mice underwent transcardial perfusion with ice-cold 0.9% saline followed by 4% paraformaldehyde (PFA). We obtained images of signal expression using a confocal microscope (FV3000, Olympus). Animals with missed injections were excluded from data analysis in this part.

Optogenetic and chemogenetic manipulation

Following optogenetic viral injections, we implanted an optic fiber into the SIHL or S2 of anesthetized mice. We used tissue glue and dental cement to firmly attach the embedded optical fiber to the skull. The embedded fibers, with a diameter of 200 μm (Newdoon, China), were connected using optic fiber sleeves to a laser generator. Mice were allowed to recover for at least 2 weeks before the experiment. We handled the mice daily for at least 3 days before behavioral experiments. On the day of the experiment, we anesthetized the mice with isoflurane to connect the chronically implanted fibers, with a diameter of 200 μm (Newdoon), to a laser generator using optic fiber sleeves. Next, we delivered yellow light (594 nm, 5–8 mW, constant), controlled by a Master-8 pulse stimulator (A.M.P.I.), for optogenetic inhibition. For chemogenetic manipulation, mice received intraperitoneal injections of the chemical ligand CNO (5 mg/kg, Sigma) under isoflurane anesthesia. Behavior tests were conducted 30 minutes later.

Microendoscope imaging

Three weeks after virus infection and GRIN lens implantation, we attached a miniature fluorescent microscope (Inscopix, USA) to the baseplate of the GRIN lens. The mice acclimatized to the weight of the lens in a freely movable test chamber for 15 minutes three times a day before formal data collection. We recorded final data for 10 minutes before the CFA mice received the capsaicin injection as a baseline, and then recorded for 10 minutes after the capsaicin injection. After chemogenetic inhibition of the contralateral S2 or S2 neurons, we recorded final data for 10 minutes before the mice received the CNO injection as a baseline, and then recorded for 10 minutes after the CNO injection.

To ensure tracking of the same neurons across different time points, longitudinal registration was conducted using Inscopix software and a custom script in MATLAB, as previously described⁵⁵. This method utilizes a probabilistic approach based on the centroid distance of adjacent cell pairs from different time periods and the Pearson correlation between their spatial footprints to determine whether they represent the same entity.

The raw Ca^{2+} data underwent preprocessing using Mosaic software (Inscopix) and custom-written scripts in MATLAB as previously

described¹² (<https://github.com/mukamel-lab/CellSort>). In brief, the imaging data were $2\times$ temporally down-sampled and corrected for motion using the default settings within the software. Subsequently, the detected fluorescence signals were normalized by their time averaged mean value ($\Delta F/F$ calculation), followed by standard Principal Component Analysis (PCA)/Independent Component Analysis (ICA) using the software to extract the normalized Ca^{2+} fluorescence signal associated with individual cells. Finally, putative cells were manually sorted based on $\Delta F/F$ values and the cell morphology determined from the location of the source pixel. Calcium events of the soma were identified through spike inference, with calcium values exceeding a predefined threshold. Z-score were computed as $(F(t)-F_m)/s.d.$, where $F(t)$ represents the averaged fluorescence signal value at time t , and F_m and $s.d.$ denote the mean and standard deviation of the ΔF values over a baseline period of the first 10 minutes.

Stimulus-evoked activity was assessed by aligning Ca^{2+} traces around the onset of scratching behavior or application of each mechanical stimulus. Average Ca^{2+} fluorescence traces for each trial were obtained for individual neurons by calculating the temporal Z-scores from -5 s to 10 s, wherein 0 represents the onset of stimulation. Z-scores were computed as $F(t)-F_m/s.d.$, in which $F(t)$ represents the average fluorescence signal (ΔF) intensity at time t , and F_m and $s.d.$ are the mean and standard deviation of ΔF values over the baseline period spanning -5 s to 0 s. All traces from the same experimental conditions were aligned and sorted by average change in Ca^{2+} fluorescence intensity for all the neurons. The mean activity traces were calculated by averaging trace values across of all neurons, with at least three trials for each stimulus type. Calcium events in the soma were obtained during 1 minute before and 2 minute after stimulation onset by identified through spike inference, with calcium values exceeding a predefined threshold.

In vitro electrophysiological recording

Brain slice preparation. Mice were deeply anesthetized with isoflurane, followed by intracardial perfusion with approximately 20 ml of ice-cold oxygenated N-methyl-D-glucamine artificial cerebrospinal fluid (NMDG ACSF) containing (in mM) 93 NMDG, 20 HEPES, 25 glucose, 30 NaHCO_3 , 10 MgSO_4 , 2.5 KCl, 1.2 NaH_2PO_4 , 0.5 CaCl_2 , 1.2 NaH_2PO_4 , 5 Na-ascorbate, 3 glutathione, 2 thiourea, and 3 Na-pyruvate (pH: 7.3–7.4, osmolarity: 300–305 mOsm/kg). Coronal slices (280 μm) containing the contralateral S2, S2, or SIHL were sectioned with a vibrating microtome (VT1200s, Leica, Germany) and initially incubated in oxygenated HEPES ACSF solution (28°C) containing (in mM) 20 HEPES, 25 glucoses, 92 NaCl, 2.5 KCl, 1.2 NaH_2PO_4 , 30 NaHCO_3 , 2 thiourea, 5 Na-ascorbate, 3 Na-pyruvate, 3 glutathione (GSH), 2 CaCl_2 , and 2 MgSO_4 (pH 7.3–7.4, osmolarity 300–305 mOsm/kg) for at least 1 hour. Subsequently, the brain slices were transferred to a slice chamber (Warner Instruments, USA) for whole-cell recording and continuously perfused with oxygenated standard ACSF solution (32°C) containing (in mM) 3 HEPES, 10 glucoses, 129 NaCl, 3 KCl, 2.4 CaCl_2 , 1.3 MgSO_4 , 1.2 KH_2PO_4 , and 20 NaHCO_3 (pH: 7.3–7.4, osmolarity: 300–310 mOsm/kg) at a rate of 2.5–3 ml/min. The temperature of the standard ACSF solution was maintained with an in-line solution heater (TC-344B, Warner Instruments, USA).

Whole-cell patch-clamp recordings. Neurons in regions of interest were visualized using a water immersion objective ($\times 40$) on an upright microscope (BX51WI, Olympus, Japan) equipped with interference contrast (IR/DIC) and an infrared camera connected to the video monitor. Whole-cell patch-clamp recordings were performed from visually identified contralateral S2, S2, or SIHL neurons. Patch pipettes were pulled from borosilicate glass capillaries (outer diameter, 1.5 mm, VitalSense Scientific Instruments Co., Ltd., Wuhan, China) using a four-stage horizontal puller (P1000, Sutter Instruments, USA). Signals were acquired after low-pass filtering at 2.8 kHz and digitized at 10 kHz using a

Multiclamp 700B amplifier. Data were collected from neurons with appropriate input resistance (more than 100 M Ω) and series resistance (less than 30 M Ω) using Clampex 10 (Molecular Devices, Sunnyvale, CA).

Light-evoked response. Optical stimulation was conducted using a laser (Shanghai Fiblaser Technology Co., Ltd., China) through an optical fiber (diameter, 200 μ m, Newdoon, China) positioned 0.2 mm above the surface of the target brain region. To validate the function of the AAV-DIO-ChR2-mCherry virus, mCherry-labeled neurons expressing ChR2 in *Fos*^{TRAP2} mice were visualized and subjected to blue laser light. EPSCs were recorded at -70 mV following photo-stimulation of ChR2-expressing contralateral S2 neuronal fibers in the S2 slices. IPSCs were recorded at 0 mV after photo-stimulation of ChR2-expressing S2 neuronal fibers in the SIHL slices.

Immunohistochemistry and imaging

First, we deeply anesthetized the mice using isoflurane. Subsequently, they were perfused with ice-cold 0.9% saline and 4% paraformaldehyde (PFA). The brains were carefully extracted and placed in PBS containing 4% PFA at 4 °C for overnight storage. They were then incubated in 20% (w/v) sucrose until they sank, followed by 30% (w/v) sucrose until they sank. Coronal slices were cut to a thickness of 40 μ m using a cryostat (Leica CMI860). For immunofluorescence, the sections were incubated with blocking buffer (0.5% Triton X-100, 5% donkey serum in PBS) for 1 hour at room temperature. Subsequently, the slices were treated with primary antibodies diluted in blocking solution, including anti-DsRed (1:200, rabbit, Takara), anti-glutamate (1:500, rabbit, Sigma), anti-GABA (1:500, rabbit, Sigma), anti-c-Fos (1:1000, rabbit, Cell Signaling Technology), anti-CUX-1 (1:500, rabbit, Atlas), and anti-NECAB1 (1:500, rabbit, Proteintech) at 4 °C for 24 hours. After washing with PBS three times for 5 minutes each, the slices were incubated with the corresponding fluorophore-conjugated secondary antibodies (1:500, Invitrogen) for 1.5 hours at room temperature. Finally, the slices were incubated in 4,6-diamidino-2-phenylindole (DAPI; 1:2000, Sigma) in the last stage. The fluorescence signals were visualized by scanning and imaging the slices with a FV3000 microscope.

To compare brightfield image data from immunohistochemistry (IHC) analysis with tdTomato signals, IHC was conducted in the same slices after obtaining fluorescence signal data^{56,57}. In detail, after capturing fluorescence images, slices were washed with running water until clear. Then, antigen retrieval was performed by submerging slices in citrate buffer (pH 6.0), followed by 10 min incubation in 3% hydrogen peroxide at room temperature. Slices were then rinsed 3 times in PBS, blocked with primary anti-c-Fos antibodies (1:1000, rabbit, Cell Signaling Technology) for 10 min and incubated at 4 °C overnight. Sections were then rinsed with PBS three times and incubated with streptavidin peroxidase and biotinylated goat anti-polyvalent antibody. DAB staining was used to visualize antibody signal, hematoxylin was used to stain nuclei, and lithium carbonate solution was used to add blue tint. Positively stained sections were converted to brown by transillumination under the microscope and negative controls comprised slices that were incubated without primary antibody. An Olympus BX43 light microscope (Olympus, Japan) was used to examine stained sections and Photoshop (CS6, Adobe) was used to register IHC signal from brightfield micrographs onto tdTomato fluorescence images.

Tissue clarity and morphological reconstruction

The mice brain was cleared using the CLARITY method with the Polymerization and electrophoresis cleaning equipment (Logos System), 12.5 mg of the polymerization initiator was added to a centrifuge tube containing 5 ml hydrogel solution and mixed thoroughly.

The whole brain was immersed in the mixture and placed in a refrigerator at 4 °C for 24 hours. Subsequently, the centrifuge tube, with the lid removed, was placed in the polymerization system to react for 3 hours at 37 °C and 90 kPa. Following this, the brain was extracted and eluted three times with PBS for 1 hour each. The brain was then subjected to the electrophoresis cleaning system at 37 °C for 10 hours with a current of 1.2 A and a peristaltic pump speed of 100 rpm. The sample underwent cleaning with 1 \times PBS for 3 hours at 30-minute cycles in a 37 °C constant temperature shaker (40 rpm). Finally, the sample was immersed in 5 mL mounting solution at 37 °C and 40 rpm. After 8 hours, the sample was transferred to 10 mL fresh mounting solution for refractive index matching and left overnight. The cleared brain was imaged using Zeiss Lightsheet 7, equipped with two-sided $\times 5/0.1$ NA illumination optics and $\times 5/0.16$ NA detection optic, and the images were analyzed using Imaris software.

Statistics and reproducibility

GraphPad Prism 8 (GraphPad Software, Inc., USA) was used for analyses and graphing. Offline analyses of data from electrophysiological recordings were conducted using Clampfit software version 10.7 (Axon Instruments, Inc., USA). Inscopix data processing software (version 1.1.6) was employed for offline analyses of data from microendoscope recordings. For representative images and statistical data, each experiment has been repeated in at least three mice with multiple brain slices in the manuscript with consistent results. Whole-brain imaging experiments were performed 5 independent times (1 animal per group) with similar results.

The Shapiro-Wilk test was used to check the normality of data. A Nonparametric Mann-Whitney *U* test or Wilcoxon matched-paired signed rank test was performed if data were not normally distributed. We performed paired or unpaired two-tailed Student's *t*-tests to compare data between two groups. For experimental groups with multiple comparisons, we utilized two-way ANOVA followed by post hoc analyses. Significance levels were indicated as **P* < 0.05, ***P* < 0.01, and ****P* < 0.001. *P* values less than 0.0001 are not provided as exact values. All results are presented as means \pm SEM. All the statistical tests, significance analyses, number of individual experiments, and other relevant information for data comparison are specified in Supplementary Data 2.

Reporting summary

Further information on research design is available in the Nature Portfolio Reporting Summary linked to this article.

Data availability

All data necessary to understand and assess the conclusions of this study are available in the main text or the supplementary materials. There are no restrictions on data availability in the manuscript. Source data are provided with this paper.

Code availability

Tracking of the same neurons across different time points, longitudinal registration was conducted using Inscopix software as described in ref. 55 and readily available at <https://github.com/zivlab/CellReg>. Raw Ca²⁺ data were preprocessed using Inscopix software and custom-written scripts in MATLAB as described in ref. 12 and available at <https://github.com/mukamel-lab/CellSort>.

References

1. Moont, R. et al. Pain inhibits pain' mechanisms: is pain modulation simply due to distraction? *Pain* **150**, 113–120 (2010).
2. Defrin, R. et al. The interactions between spatial summation and DNIC: effect of the distance between two painful stimuli and attentional factors on pain perception. *Pain* **151**, 489–495 (2010).

3. Nahman-Averbuch, H. & I. Timmers. Neural mechanisms underlying the conditioned pain modulation response: a narrative review of neuroimaging studies. *Pain* **164**, e25–e46 (2023).
4. Le Bars, D., Dickenson, A. H. & Besson, J. M. Diffuse noxious inhibitory controls (DNIC). I. Effects on dorsal horn convergent neurones in the rat. *Pain* **6**, 283–304 (1979).
5. Le Bars, D., Dickenson, A. H. & Besson, J. M. Diffuse noxious inhibitory controls (DNIC). II. Lack of effect on non-convergent neurones, supraspinal involvement and theoretical implications. *Pain* **6**, 305–327 (1979).
6. Tobaldini, G. et al. Pain inhibits pain: an ascending-descending pain modulation pathway linking mesolimbic and classical descending mechanisms. *Mol. Neurobiol.* **56**, 1000–1013 (2019).
7. Wen, Y. R. et al. DNIC-mediated analgesia produced by a supra-maximal electrical or a high-dose formalin conditioning stimulus: roles of opioid and alpha2-adrenergic receptors. *J. Biomed. Sci.* **17**, 19 (2010).
8. Schmidt, B. L. et al. Adaptations in nucleus accumbens circuitry during opioid withdrawal associated with persistence of noxious stimulus-induced antinociception in the rat. *J. Pain.* **4**, 141–147 (2003).
9. Huang, J. et al. A neuronal circuit for activating descending modulation of neuropathic pain. *Nat. Neurosci.* **22**, 1659–1668 (2019).
10. Tan, L. L. & Kuner, R. Neocortical circuits in pain and pain relief. *Nat. Rev. Neurosci.* **22**, 458–471 (2021).
11. Zhang, M. et al. Cortical regulation of helping behaviour towards others in pain. *Nature* **626**, 136–144 (2024).
12. Liu, Y. et al. Touch and tactile neuropathic pain sensitivity are set by corticospinal projections. *Nature* **561**, 547–550 (2018).
13. Wali, M. Role of the somatosensory cortex in motor memory consolidation. *J. Neurophysiol.* **124**, 648–651 (2020).
14. Buetfering, C. et al. Behaviorally relevant decision coding in primary somatosensory cortex neurons. *Nat. Neurosci.* **25**, 1225–1236 (2022).
15. Romo, R. et al. Neuronal correlates of decision-making in secondary somatosensory cortex. *Nat. Neurosci.* **5**, 1217–1225 (2002).
16. Kumar, N., Manning, T. F. & Ostry, D. J. Somatosensory cortex participates in the consolidation of human motor memory. *PLoS Biol.* **17**, e3000469 (2019).
17. Manita, S. et al. A top-down cortical circuit for accurate sensory perception. *Neuron* **86**, 1304–1316 (2015).
18. Condylis, C. et al. Context-dependent sensory processing across primary and secondary somatosensory cortex. *Neuron* **106**, 515–525.e5 (2020).
19. Yu, Y. et al. Layer-specific activation of sensory input and predictive feedback in the human primary somatosensory cortex. *Sci. Adv.* **5**, eaav9053 (2019).
20. Okada, T. et al. Pain induces stable, active microcircuits in the somatosensory cortex that provide a therapeutic target. *Sci. Adv.* **7**, eabd8261 (2021).
21. Ziegler, K. et al. Primary somatosensory cortex bidirectionally modulates sensory gain and nociceptive behavior in a layer-specific manner. *Nat. Commun.* **14**, 2999 (2023).
22. Li, Z. et al. Locating causal hubs of memory consolidation in spontaneous brain network in male mice. *Nat. Commun.* **14**, 5399 (2023).
23. Rossi-Pool, R. et al. A continuum of invariant sensory and behavioral-context perceptual coding in secondary somatosensory cortex. *Nat. Commun.* **12**, 2000 (2021).
24. Gan, Z. et al. Layer-specific pain relief pathways originating from primary motor cortex. *Science* **378**, 1336–1343 (2022).
25. Szczot, M. et al. PIEZO2 mediates injury-induced tactile pain in mice and humans. *Sci. Transl. Med.* **10**, eaat9892 (2018).
26. Darian-Smith, I., Rowe, M. J. & Sessle, B. J. Tactile stimulus intensity: information transmission by relay neurons in different trigeminal nuclei. *Science* **160**, 791–794 (1968).
27. Milligan, E. D. & Watkins, L. R. Pathological and protective roles of glia in chronic pain. *Nat. Rev. Neurosci.* **10**, 23–36 (2009).
28. Smith, M. L., Asada, N. & Malenka, R. C. Anterior cingulate inputs to nucleus accumbens control the social transfer of pain and analgesia. *Science* **371**, 153–159 (2021).
29. Pan, Q. et al. Representation and control of pain and itch by distinct prefrontal neural ensembles. *Neuron* **111**, 2414–2431.e7 (2023).
30. Mu, D. et al. A central neural circuit for itch sensation. *Science* **357**, 695–699 (2017).
31. Wang, L.-H., Ding, W.-Q. & Sun, Y.-G. Spinal ascending pathways for somatosensory information processing. *Trends Neurosci.* **45**, 594–607 (2022).
32. Lu, J. et al. Somatosensory cortical signature of facial nociception and vibrotactile touch-induced analgesia. *Sci. Adv.* **8**, eabn6530 (2022).
33. Allen, W. E. et al. Thirst-associated preoptic neurons encode an aversive motivational drive. *Science* **357**, 1149–1155 (2017).
34. Guenther, Casey J. et al. Permanent genetic access to transiently active neurons via TRAP: targeted recombination in active populations. *Neuron* **78**, 773–784 (2013).
35. Okada, T. et al. Pain induces stable, active microcircuits in the somatosensory cortex that provide a therapeutic target. *Sci. Adv.* **7**, eabd8261.
36. Chang, C. W. et al. A cortico-cortical pathway targets inhibitory interneurons and modulates paw movement during locomotion in mice. *J. Neurosci.* **42**, 44–57 (2022).
37. Wang, Y. et al. A frontal transcallosal inhibition loop mediates interhemispheric balance in visuospatial processing. *Nat. Commun.* **14**, 5213 (2023).
38. Peirs, C. & Seal, R. P. Neural circuits for pain: recent advances and current views. *Science* **354**, 578–584 (2016).
39. Chung, K. & Deisseroth, K. CLARITY for mapping the nervous system. *Nat. Methods* **10**, 508–513 (2013).
40. Guo, F. et al. Secondary somatosensory cortex glutamatergic innervation of the thalamus facilitates pain. *Pain* **165**, 1142–1153 (2024).
41. Taub, D. G. et al. The secondary somatosensory cortex gates mechanical and heat sensitivity. *Nat. Commun.* **15**, 1289 (2024).
42. Zhou, H. et al. A sleep-active basalocortical pathway crucial for generation and maintenance of chronic pain. *Nat. Neurosci.* **26**, 458–469 (2023).
43. Ning, L. et al. Chronic constriction injury induced long-term changes in spontaneous membrane-potential oscillations in anterior cingulate cortical neurons in vivo. *Pain. Physician* **16**, E577–E589 (2013).
44. Pala, A. & Stanley, G. B. Ipsilateral stimulus encoding in primary and secondary somatosensory cortex of awake mice. *J. Neurosci.* **42**, 2701–2715 (2022).
45. Ocklenburg, S. & Guo, Z. V. Cross-hemispheric communication: Insights on lateralized brain functions. *Neuron* **112**, 1222–1234 (2024).
46. Choi, S. et al. Parallel ascending spinal pathways for affective touch and pain. *Nature* **587**, 258–263 (2020).
47. Staud, R. et al. Diffuse noxious inhibitory controls (DNIC) attenuate temporal summation of second pain in normal males but not in normal females or fibromyalgia patients. *Pain* **101**, 167–174 (2003).
48. Huang, T. et al. Identifying the pathways required for coping behaviours associated with sustained pain. *Nature* **565**, 86–90 (2019).
49. Cheng, L. et al. Identification of spinal circuits involved in touch-evoked dynamic mechanical pain. *Nat. Neurosci.* **20**, 804–814 (2017).
50. Gu, X. et al. Neurons in the caudal ventrolateral medulla mediate descending pain control. *Nat. Neurosci.* **26**, 594–605 (2023).
51. Jourdan, D. et al. A new automated method of pain scoring in the formalin test in rats. *Pain* **71**, 265–70 (1997).
52. Jones, B. J. & Roberts, D. J. A rotarod suitable for quantitative measurements of motor incoordination in naive mice. *Naunyn Schmiedebergs Arch. Exp. Pathol. Pharmacol.* **259**, 211 (1968).
53. Kuraishi, Y. Methods for preclinical assessment of antipruritic agents and itch mechanisms independent of mast-cell histamine. *Biol. Pharm. Bull.* **38**, 635–644 (2015).

54. Hagiwara, K., Nojima, H. & Kuraishi, Y. Serotonin-induced biting of the hind paw is itch-related response in mice. *Pain. Res.* **14**, 53–59 (1999).
55. Sheintuch, L. et al. Tracking the same neurons across multiple days in Ca²⁺ imaging data. *Cell Rep.* **21**, 1102–1115 (2017).
56. Chen, C. L. et al. Runx1 determines nociceptive sensory neuron phenotype and is required for thermal and neuropathic pain. *Neuron* **49**, 365–377 (2006).
57. Liu, S. et al. A neuroanatomical basis for electroacupuncture to drive the vagal-adrenal axis. *Nature* **598**, 641–645 (2021).

Acknowledgements

This work was supported by the National Key Research and Development Program of China (STI2030-Major Projects 2021ZD0203100 to Z.Z.), the National Natural Science Foundation of China (grants 32025017 to Z.Z., 32241013 to Z.Z., 32121002 to Z.Z., 32422035 to X.Z., 32371045 to X.Z. and 323B2031 to W.D.), the Plans for Major Provincial Science & Technology Projects (202303a07020002 to Z.Z.), the Institute of Health and Medicine (QYZD20220007 to Z.Z.), the China National Postdoctoral Program for Innovative Talents (BX20240346 to W.D.) and the USTC Research Funds of the Double First-Class Initiative (YD9100002041 to X.Z., YD9110002015 to J.L., YD9110002039 to D.W.).

Author contributions

J.H., Y.J., and W.D. designed the studies, conducted most of the experiments and data analysis, and wrote the draft manuscript. P.C. and J.M. conducted some of the behavioral experiments. W.Z., A.L., and D.W. conducted the behavioral experiments and data analyses and wrote the text of the final manuscript. J.L. and W.T. were involved in the overall design of the study, and X.Z. and Z.Z. were involved in the overall design of the project, individual experiments, data analysis, and the writing of the final manuscript.

Competing interests

The authors declare no competing interests.

Additional information

Supplementary information The online version contains supplementary material available at <https://doi.org/10.1038/s41467-025-57050-y>.

Correspondence and requests for materials should be addressed to Zhi Zhang, Wenjuan Tao or Xia Zhu.

Peer review information *Nature Communications* thanks Hiroaki Wake, and the other, anonymous, reviewers for their contribution to the peer review of this work. A peer review file is available.

Reprints and permissions information is available at <http://www.nature.com/reprints>

Publisher's note Springer Nature remains neutral with regard to jurisdictional claims in published maps and institutional affiliations.

Open Access This article is licensed under a Creative Commons Attribution-NonCommercial-NoDerivatives 4.0 International License, which permits any non-commercial use, sharing, distribution and reproduction in any medium or format, as long as you give appropriate credit to the original author(s) and the source, provide a link to the Creative Commons licence, and indicate if you modified the licensed material. You do not have permission under this licence to share adapted material derived from this article or parts of it. The images or other third party material in this article are included in the article's Creative Commons licence, unless indicated otherwise in a credit line to the material. If material is not included in the article's Creative Commons licence and your intended use is not permitted by statutory regulation or exceeds the permitted use, you will need to obtain permission directly from the copyright holder. To view a copy of this licence, visit <http://creativecommons.org/licenses/by-nc-nd/4.0/>.

© The Author(s) 2025